UCRL--53354

DE83 006305

UCRL-53354
Distribution Category UC-4, 25

The Hydrides of $CeNi_5$, $MmNi_5$, $Ca_{0.2}(Ce_{0.65}Mm_{0.35})_{0.8}Ni_5$, $Ca_{0.2}Ce_{0.8}Ni_5$, $Ca_{0.2}Mm_{0.8}Ni_5$, and Mixed $CeNi_5/MmNi_5$

J. F. Lakner

T. S. Chow

Manuscript date: September 1982

LAWRENCE LIVERMORE LABORATORY
University of California • Livermore, California • 94550

Available from: National Technical Information Service • U.S. Department of Commerce
5285 Port Royal Road • Springfield, VA 22161 • $8.50 per copy • (Microfiche $4.50)

Contents

The Hydrides of $CeNi_5$, $MmNi_5$, $Ca_{0.2}(Ce_{0.65}Mm_{0.35})_{0.8}Ni_5$, $Ca_{0.2}Ce_{0.8}Ni_5$, $Ca_{0.2}Mm_{0.8}Ni_5$, and Mixed $CeNi_5/MmNi_5$

Abstract

Six intermetallic alloys [$CeNi_5$, $MmNi_5$, $Ca_{0.2}(Ce_{0.65}Mm_{0.35})_{0.8}Ni_5$, $Ca_{0.2}Ce_{0.8}Ni_5$, $Ca_{0.2}Mm_{0.8}Ni_5$, and a mixed alloy, $CeNi_5/MmNi_5$] were investigated with respect to their suitability to provide high hydrogen capacity and their potential for use in providing substantial hydrogen pressure at both low and high temperatures. A second phase of our investigation dealt with ball-milling and hydriding and dehydriding cycles to produce fine particles for use in hydride powder transfer studies.

A summary of several Van't Hoff plots is also included for hydride-forming alloys.

Introduction

The purpose of our study was to select metal hydrides which would supply substantial hydrogen pressure at sub-zero temperatures, and at the same time, possess a high hydrogen capacity. Obviously, the stable hydrides (e.g., ZrH_2 and LiH) are ruled out. Very stable hydrides require a high temperature (up to 1000°C) for the reverse reaction to take place at 1 atm. At above-ambient temperatures, those hydrides suitable for low temperatures would naturally be satisfactory in supplying hydrogen pressure, in some cases, at more than substantial pressures. The pressure is different for different hydrides. It was also desirable to have a low ΔH_f (slope of Van't Hoff plot*) so that sub-zero and above-ambient pressure differences would not be large. Other properties of importance are (1) rate of sorption (kinetics of reaction), (2) constancy of the equilibrium pressure, (3) a long, flat plateau, and (4) insensitivity to impurities. In addition to selecting suitable hydrides, we also wished to study hydrogen powder transfer through tubing so that the hydride could deliver its hydrogen at a remote source. For this study, the particle-size characteristics needed to be determined. Since virtually all applications exploit the fact that hydrogen can be stored in a compact form, it is appropriate to compare hydrogen density in some hydrogen compounds. These are listed in Table 1.[1]

* Van't Hoff plot shows dissociation pressures plotted vs 1/T.

Studies of hydrogen sorption by intermetallic compounds and alloys were reported only intermittently until the early 1960s. Most of this early work dealt with alloys of palladium and platinum, nickel, copper, and especially silver.

From 1961 through 1962, the Denver Research Institute published hydrogen adsorption measurements.[2] Although many of these measurements have since been refuted and additional compounds having high hydrogen solubility have been found, these studies were the first large-scale investigations of hydrogen interaction with intermetallic compounds.

A literature review of metallic ternary and quarternary hydrides published by Newkirk covers a wide range of alloys and intermetallic compounds which have been examined recently.[3]

We also made an initial survey of the literature of isotherms and Van't Hoff plots to determine if any were suitable for our work. The results of our limited survey are shown in Figs. 35 and 36 in Appendix A, and also in References 4 through 37.

It is rather difficult to predict whether alloys or intermetallic compounds will absorb hydrogen. There is no theory available which relates alloy composition to hydriding and dehydriding (hereafter written as hydriding-dehydriding), although some rules have been developed of which Miedema's "Reversed Stability" rule is the most notable.[38] It has been useful in studies of AB_5 alloys.

Table 1. Comparison of the hydrogen contents in various hydrogen compounds.[a]

Compound	Molecular wt (kg/kmole)	Density (kg/m^3)	No. H atoms/ unit volume ($\times 10^{28}/m^3$)	Wt % H_2	Partial H_2 density (kg/m^3)
H_2O	18	1000	6.7	11	111
H_2SO_4	98.1	1841	2.2	2	36
liq. CH_4	16.0	425	6.3	25	105
TiH_2	49.9	3900	9.2	4	153
ZrH_2	93.2	5610	7.3	2.1	122
YH_2	90.9	3958	5.7	2.2	95
LaH_2	140.9	5120	4.4	1.4	73
LaH_3	141.9	5350	6.5	2.1	108
$LaNi_5H_6$	438.5	6225	5.3	1.4	88
$TiFeH_{1.98}$	105.7	5470	6.2	1.85	101
LiH	100				100

[a] $LaNi_5$ has a density of 8,300 kg/m^3, the hydride $LaNi_5H_6$ powder has a bulk density of 3,200 kg/m^3. Therefore, $N_H = 2.7 \times 10^{28}$ atoms H/m^3, the partial H_2 density = 45 kg/m^3 which represents a potential H_2 pressure = 780 atm at 0°C.

In addition, one wishes to confirm those literature values because of shifts in isotherms due to impurities, slight variations in composition and variations from batch to batch of material.

Apparatus, Materials and Procedures

Pressuring System

The hydrogen-pressuring system used for our studies was constructed of 316 and A-286 stainless-steel alloys. Where these steels were used as vessel liners only, an AISI 4340 steel outer cylinder provided additional strength. Figure 1 shows a schematic drawing of the apparatus. It is capable of handling pressurized hydrogen up to 6,800 atm at temperatures up to 200°C and down to −55°C.

The pressure transducers used were Teledyne Taber models 2404, 1205 and 1207. The choice depended upon the pressure range in which the hydriding occured. Experiments involving very high pressures relied on a Precise Sensors Corporation unit or an Astra Corporation unit. (Manganin coils could also be used provided they were isolated from the hydrogen.) A low-pressure transducer at approximately 13 atm (200 psi) was used during the initial phase of the experiment to obtain maximum sensitivity. For low-temperature runs, pressure transducers were placed outside the cold zone and connected with 0.127-mm i.d. tubing.

Hydrogen for use in these experiments was purified by passing it over a molecular sieve cooled by liquid nitrogen; it was then compressed into storage bottles at 1,677 atm. Figure 2 shows the charging system at (a); the hydriding vessel is situated behind the wall on the right. The desorption bottles are located at (b). The free-void volumes of both the charging system (24.87 cm^3) and the hydriding vessel (approximately 10 cm^3) were kept low to give readings of large pressure differentials during the hydriding experiments.

Pressure Vessel

Autoclave Engineers, Inc. and Lawrence Livermore National Laboratory (LLNL) designed a double-walled pressure vessel (Fig. 3). It consists of a liner of A-286 ACQ steel (o.d. 2.54 cm) shrunk into a supporting body of AISI 4340 steel (o.d. 9.53 cm). The liner bore is 0.794 cm with 60° coned seats at each end. The short length of the vessel, approximately 50 cm, permits its handling in a glovebox for sample loading under argon gas.

Phonographic grooves on the exterior surface of the liner permit any diffused gas to reach either weep hole. The inside of the liner may be gold-plated if it is found that hydrogen losses are significant for runs above ambient temperatures.

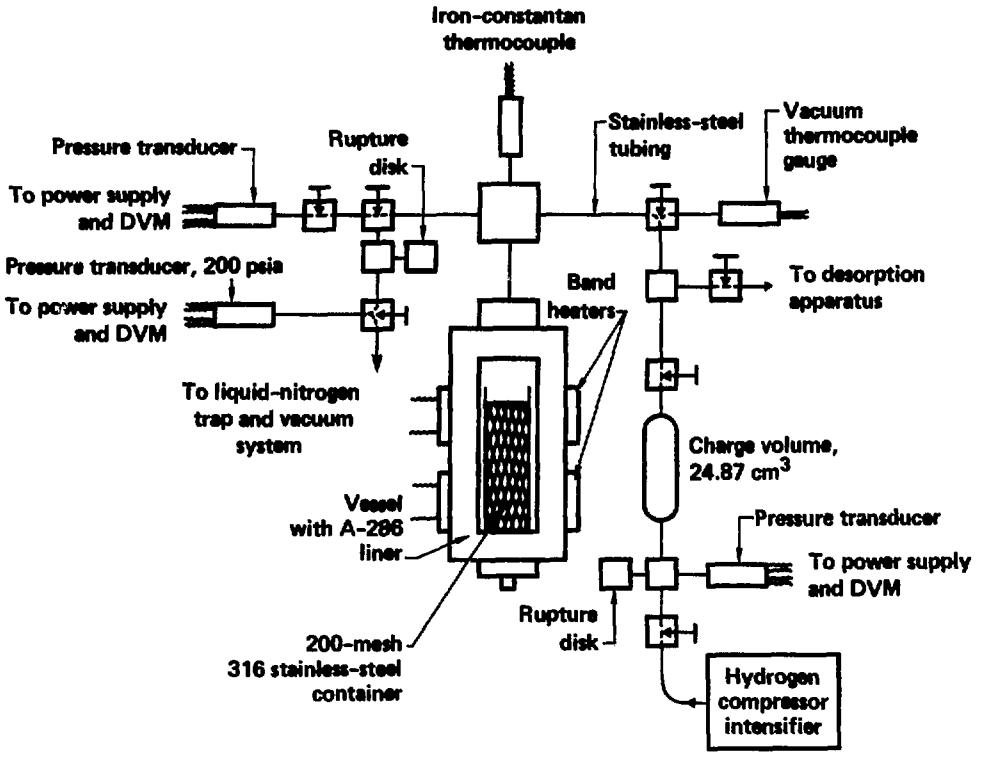

Figure 1. Schematic drawing of apparatus for hydriding to pressures up to 6,800 atm (690 MPa) and temperatures up to 200°C. For temperature runs, the pressure vessel is placed inside a Thermatron Co. refrigeration-heater unit.

The sample is contained within the pressure vessel in a 316 stainless-steel container made of 200-mesh wire or a sintered porous stainless-steel thimble. The porosity of this container permits rapid omnidirectional access of hydrogen to the sample.

Test Configuration for Hydride Powder Transfer Experiments

The test setup for hydride transfer experiments, as seen in Figs. 4 and 5, consisted primarily of the storage and the receiving reservoirs connected by a 1/8″ o.d. × 0.08″ i.d. high-pressure tubing isolable by a solenoid valve. The storage reservoir has a total storage volume of 160-cc containing a 66-cc space for the solid particulate storage as shown in Fig. 6. The partition wall contains two 0.025″ i.d. vanes to induce fluidization and mixing during transport. The vanes are fitted with short pieces of sintered stainless-steel disks to prevent the solid powder from moving into the other compartment during storage. The 60-cc compartment is capable of storing up to 210 g of metal powder, and the gaseous space volume is adjustable to allow reduction up to 100 cc by inserting a dummy mass of suitable size. Both reservoirs are instrumented to monitor both temperature and pressure data.

Test Method

The $CeNi_5$ sample was ball-milled for 16 h, hydrided-dehydrided for 12 cycles, and sifted

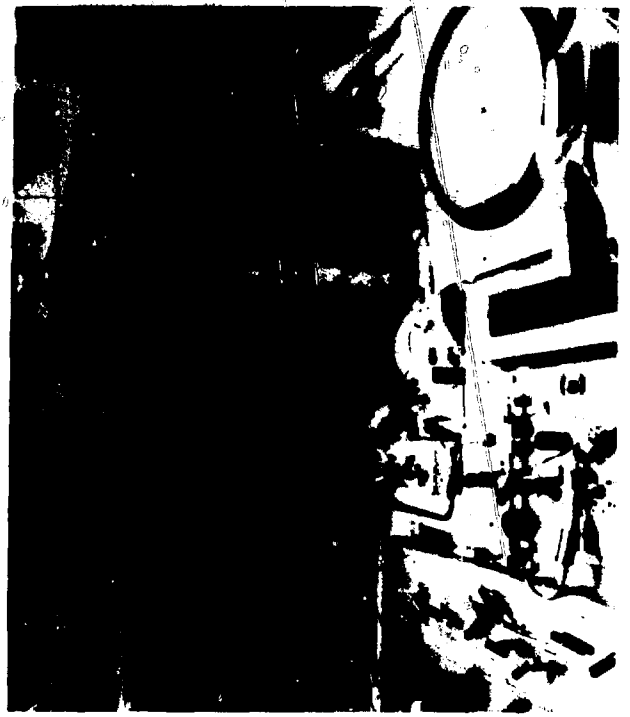

Figure 2. Instrumentation of the hydriding apparatus, including (a) the sample charging system, (b) desorption bottles and (c) digital voltmeters.

with a 400-mesh sieve. The size analysis showed the distribution to be 68% below 10 microns and essentially none above 20 microns. This size range puts the metal particles on a comparable level, in terms of the forces (gravity, buoyancy and drag) that influence the mobility of the particle, as that of 75–105 micron size zeolite particles which we had successfully transferred using the same reservoir.

We began the hydriding of a metal/alloy system by loading a sample up to 200 g into an s-s vessel. Sample loading was done under an argon atmosphere. The vessel was transferred to a hydrogen pressure vacuum system and the argon was evacuated from the vessel, after which the sample was ready for hydriding. To hydride the sample, a storage reservoir of 25 cc was repeatedly charged with hydrogen to the maximum pressure of 20,000 psig. From this reservoir, small aliquots of hydrogen were added to the sample. The pressure and temperature in both the reservoir and the sample vessel were recorded. Knowing the pressure, volume, and temperature, we could calculate the amount of hydrogen absorbed. Once the desired amount of hydrogen was reached, the sample vessel was secured. The storage reservoir (vessel "A") was then connected through a 0.08" tubing with a solenoid isolation valve to an evacuated vessel "B" of volume 1026 cc or 2247 cc (see Fig. 1). At T_0, the solenoid valve was opened allowing the free expansion of the hydrogen gas to transfer the metal hydride into vessel "B." Pressure and temperature of both vessels were recorded as the pressure between the two vessels equalized and the amount of metal hydride left behind in vessel "A" was measured.

Gaseous transfer runs were made for both the $CeNi_5$ hydride powder and pure hydrogen gas. The pure gas tests were done with a 20.75-cc aluminum dummy volume inserted in the storage reservoir to substitute for the volume of hydrides. The size of the volume was chosen to mock 200 g of $CeNi_5$ in order to provide a comparison basis on the effect of dehydriding during the free expansion process. All the tests performed so far were at room temperature.

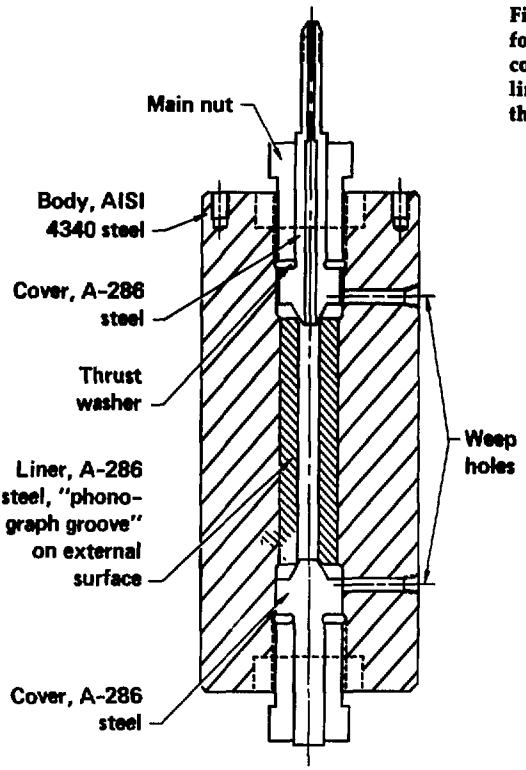

Figure 3. Details of a pressure vessel designed for the conditions of 6,800 atm and 200°C. The covers and liner are A-286 stainless steel. The liner and grooves prevent hydrogen attack on the supporting body.

Sample Preparation and Procedure

Alloy Analyses

All alloys were cast by Ergenics of Wyckoff, New Jersey in 4-kg lots. The analyses of each alloy are given in Table 2.

Photomicrographs of Alloys

Figures 7, 8, and 9 are photomicrographs of $CeNi_5$, $Ca_{0.2}Ce_{0.8}Ni_5$, and $Ca_{0.2}(Ce_{0.65}Mm_{0.35})Ni_5$ alloys, respectively. The photomicrograph of $CeNi_5$ shows no free nickel, although the atomic formula from batch T-87317 would indicate a slightly nickel-rich compound. The $CeNi_5$ alloy is nonmagnetic and fracture surfaces are shiny. This suggests that the alloy is completely single phase and is closer to the 1-5 composition than the chemistry data would indicate.

The photomicrographs of $Ca_{0.2}Ce_{0.8}Ni_5$ and of $Ca_{0.2}(Ce_{0.65}Mm_{0.35})Ni_5$ (Figs. 8 and 9) show a small amount of second phase, probably elemental nickel. Magnetic or microprobe work should confirm this.

The photomicrograph of $Ca_{0.2}Mm_{0.8}Ni_5$ was not available. According to Ergenics, this alloy contains 5–10 volume percent of a second phase, probably nickel.

Procedure

The alloy was crushed with a mortar and pestle into particles of about 100 Tyler mesh in an argon atmosphere and was introduced into the screen container made of 200-mesh wire. An iron-constantan thermocouple sheathed in 316 stainless steel was inserted into the crushed sample and both were inserted into the pressure vessel bore. Samples were typically 12 g. The assembled pressure vessel with its charge was connected to the hydriding system; argon was pumped out to 0.01 Torr with a mechanical pump connected in series with a liquid nitrogen trap. Then hydrogen was introduced into the system at 340 atm and left

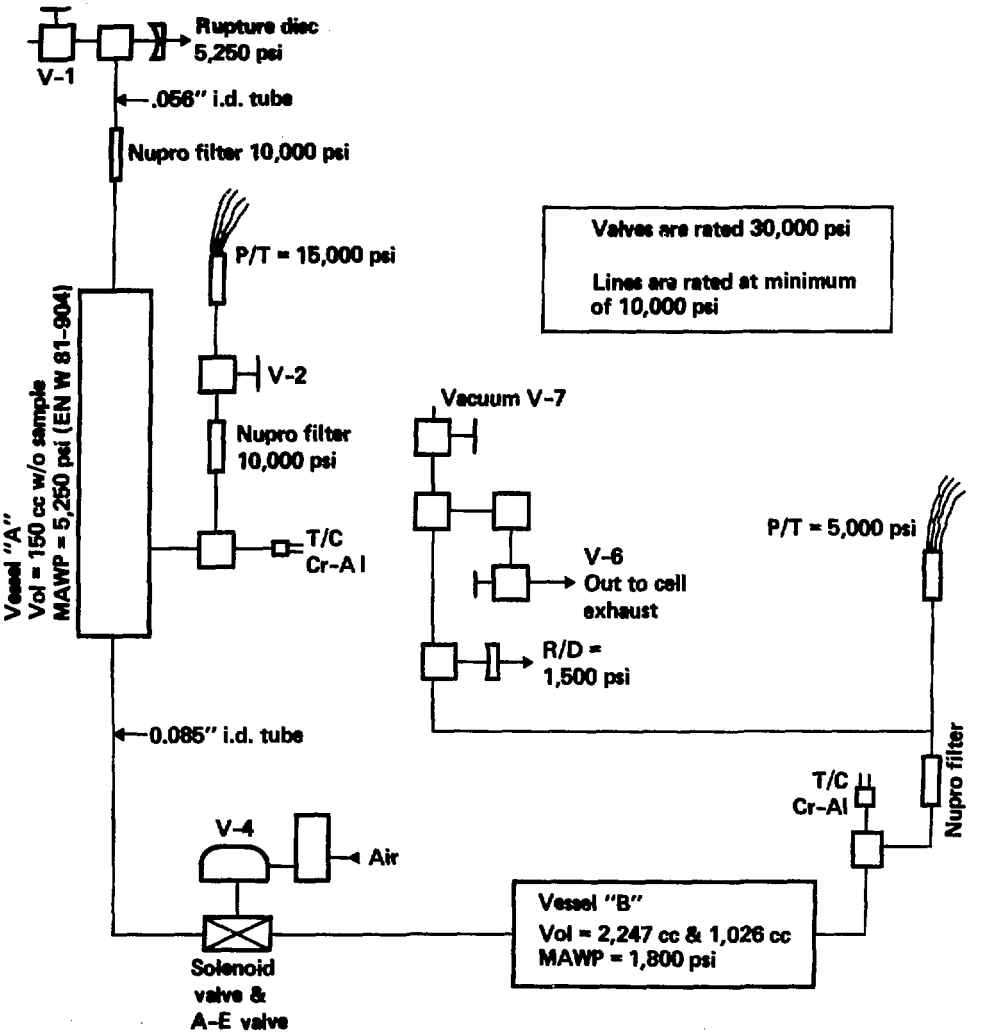

Figure 4. Schematic of experimental setup to test hydride transfer behavior.

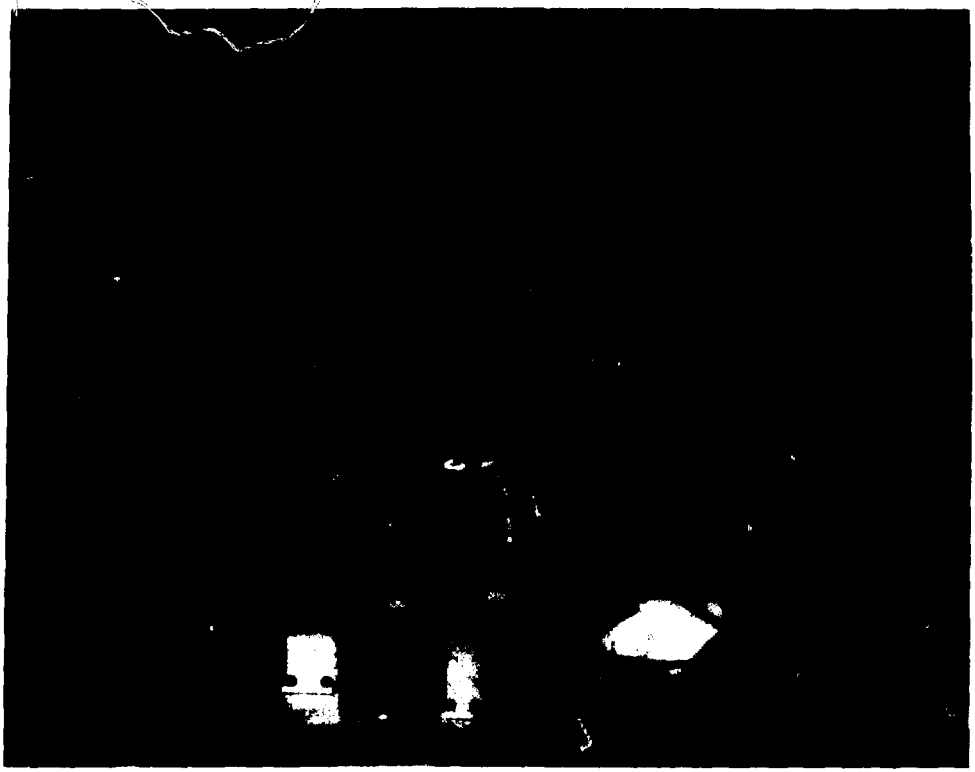

Figure 5. Hydride-powder transfer setup.

for several hours until the pressure became constant. The system was then evacuated at temperatures up to about 180 to 270°C, depending upon the alloy used. This process of activation was repeated five times before actual pressure-volume-temperature (P-V-T) measurements were taken.

Isotherms were obtained by adding or removing small aliquots of hydrogen and waiting for the pressure to stabilize. A period of 10–16 h was required to obtain a complete isotherm and assure complete equilibrium at each point.

Although $CeNi_5$ absorbs some hydrogen at room temperature, a different procedure is necessary to obtain maximum loading of the alloy $CeNi_5$. The alloy was cooled to −50°C under a pressure of 10,000 psig. Other activations were performed at ≃−20°C and greater pressures, but the threshold required for pressure and temperature has not been established. After equilibrium is established, the hydrogen pressure is released and the alloy allowed to warm up to ambient temperature. Subsequent loadings of hydrogen can be made starting at room temperature, and full loadings can be realized.

Some of our work required the production of 100–200 g batches of fine alloy powder. The alloys were ground in a 1-liter Abey ball mill, No. BF00, using 1/2″ diameter tungsten carbide balls and then exposed to several hydriding-dehydriding cycles. Particle-size analysis was done by means of the Quantamet Particle Size Analyzer. Hydrided $CeNi_5$ powders were used to study powder transfer phenomena using an overpressure of hydrogen gas.

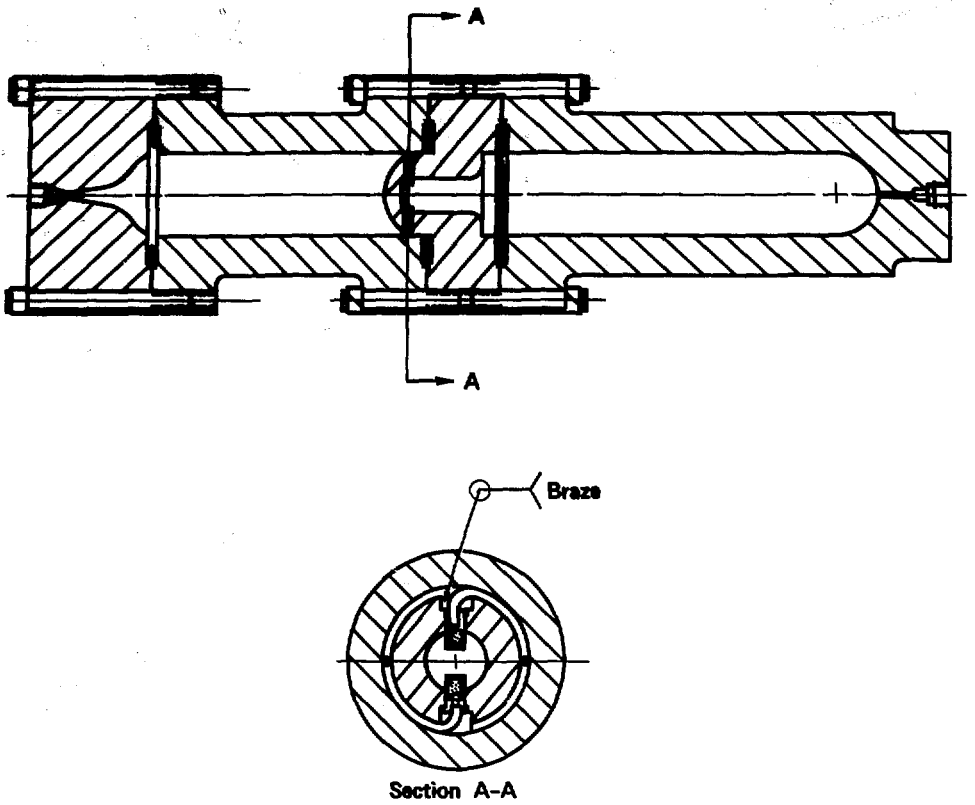

Figure 6. Hydride storage vessel for use in transfer studies.

The hydrogen/metal ratio was calculated from P-V-T measurements by a LLNL computer code which also took into account the gas compressibility factor, Z, for each condition. The volumes of absorption and desorption systems were measured using known calibrated containers attached to a Wallace and Tiernan 1500 series pressure gauge (Model 62A-4A-0045). These containers were filled with helium at a known pressure and released to the unknown volumes, both volumes, etc. being at the same temperature. A $P_1V_1 = P_2V_2$ calculation gave the unknown volume value. An isotherm was then obtained by plotting the number of atoms of hydrogen absorbed per mole of intermetallic alloy as a function of the gas pressure in atmospheres.

Table 2. Analysis of intermetallic alloys treated in this paper.

	$CeNi_5$ Ht T-87317 (wt %)	$CeNi_5$ Ht T-83583 (wt %)
Ni	67.9	68.1
Ce	31.2	31.8
O_2	0.02	0.021
Fe		0.006

	$Ca_{0.2}Mm_{0.9}Ni_5$ Ht T-84159 (wt %)	
Ni	71.7	
Ca	1.57	
Ce	26.8*	50 wt%
La		25.0
Nd		15.0
Pr		5.
Fe	.73	
O_2	.023	

* Total

	$Ca_{0.2}(Ce_{0.65}Mm_{0.35})_{0.8}Ni_5$ Ht T-85033 (wt %)
Ni	72.5
Ca	2.3
Ce	20.7
La	2.3
Nd	1.5
Pr	0.5
Fe	0.3
O_2	0.041

	$MmNi_5$ Alloy #190 Research Chemicals (1973) (wt %)
Mm	31.2-30.7
Ni	remainder
Mm*	50 (wt %) Ce
	25 (wt %) La
	15 (wt %) Nd
	3-5 (wt %) Pr
	<1 (wt %) Yt
	0.5-1 (wt %) Fe
	some Zn, Ca, Mg, Si

* Mischmetal contains a mixture of Ce, La, Nd, Pr and other rare earth metals. It is mined as monazite or bastinite ore. The Ce varies in amount in the ores.

	$Ca_{0.2}Ce_{0.8}Ni_5$ Ht T-84159 Ergenics "Hystor 203" (wt %)
Ni	73.1
Ca	2.2
Ce	24.6
O_2	0.097

	$Ca_{0.1617}Mm_{0.7884}Fe_{0.517}Ni_5$ Ht T-84159 (wt %)
Ni	70.964
Mm	25.75
Ca	1.567
Fe	0.699
O_2	0.023

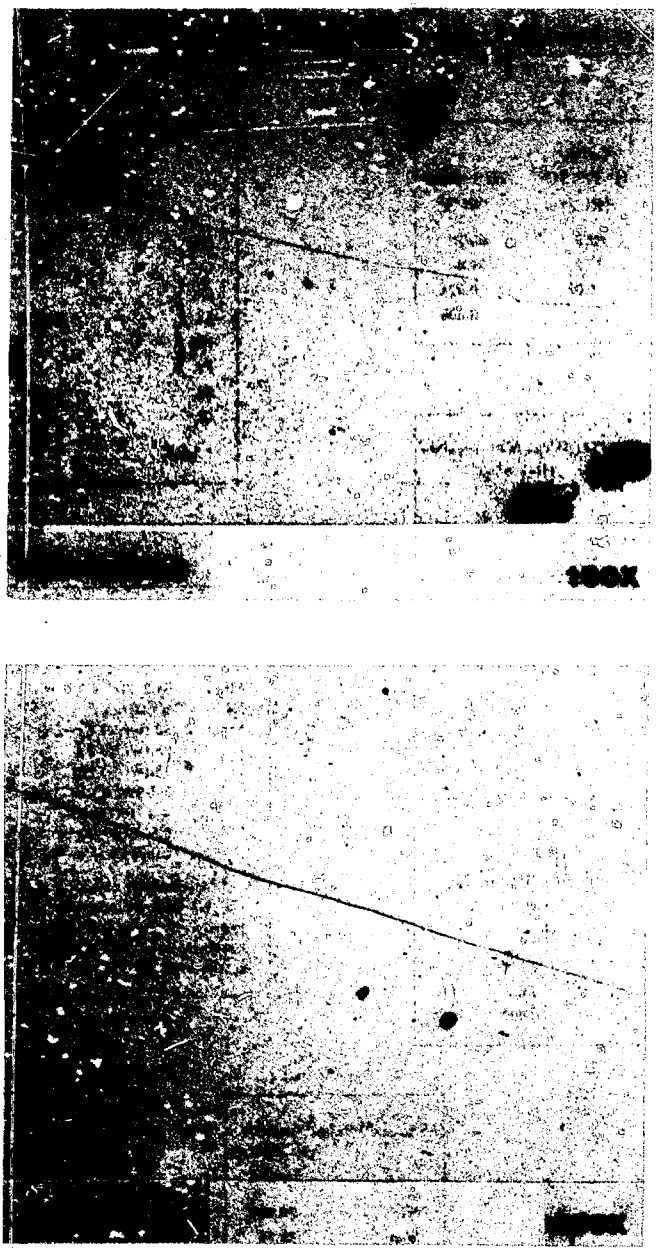

Figure 7. $CeNi_5$ photomicrograph (as cast). Merica's Etch (dilute) was used.

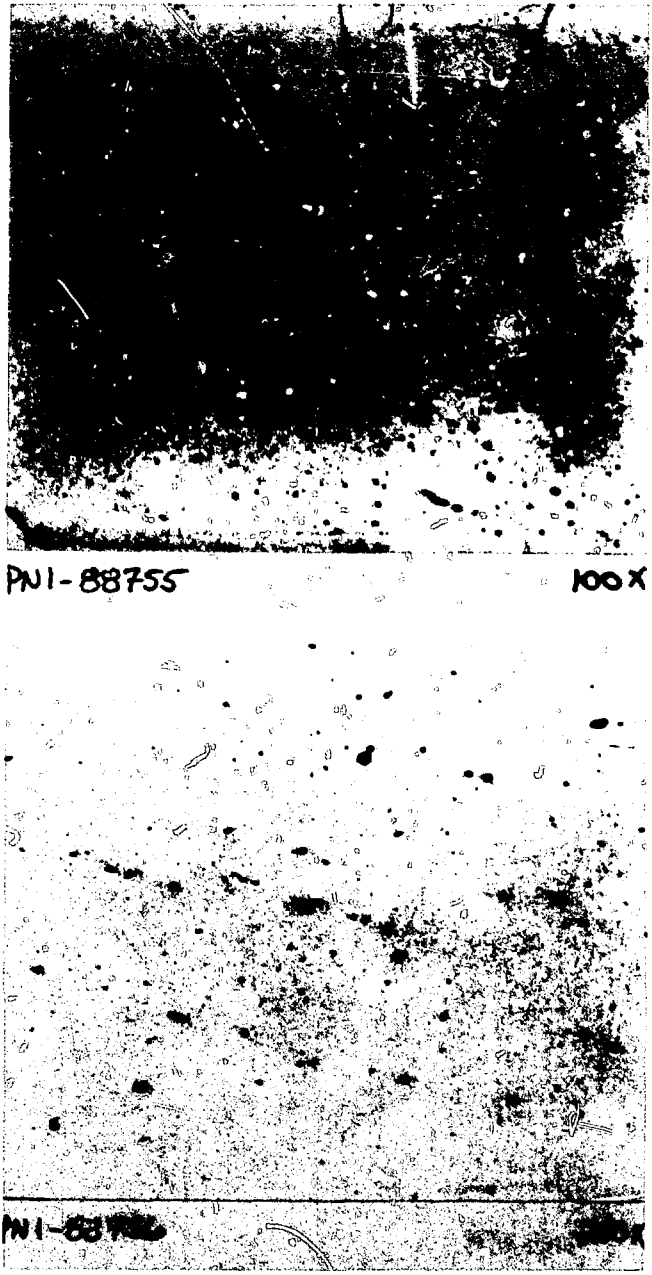

Figure 8. $Ca_{0.2}Ce_{0.8}Ni_5$ photomicrograph (as cast). Merica's Etch (dilute) was used.

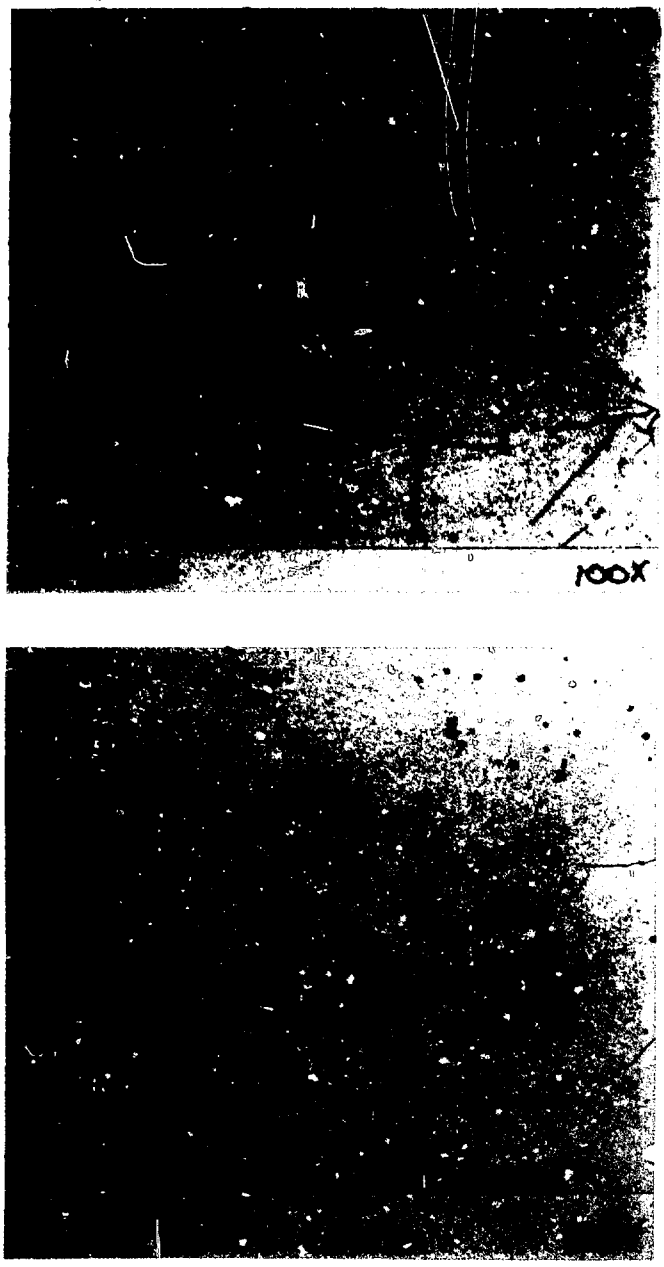

Figure 9. $Ca_{0.2}(Ce_{0.65}Mm_{0.35})_{0.8}Ni_5$ photomicrograph (as cast). Merica's Etch (dilute) was used.

Experimental Results and Discussion

Isotherms

Hydrogen absorption-desorption isotherms are the source of much of the data needed to select metallic hydrides for engineering purposes. From these isotherms, one obtains plateau pressures. They represent a composition range in which metal alloy and metal hydride phases coexist; thermodynamics suggest that the isotherms should be flat over this range. Also obtainable from the isotherms are hydrogen capacity at temperature, the slope of the plateau, and the hysteresis. The amount of slope varies from alloy to alloy and usually arises from chemical segregation during solidification. Annealing* can reduce the amount of slope.[39] A flat slope is desirable in that it allows delivery of hydrogen at a constant pressure over a composition range. A sloped plateau allows direct determination of the amount of hydrogen left in a hydride container by simply reading the pressure and temperature. This method cannot be used for a hydride with a zero plateau slope because the hydrogen/metal ratio cannot be determined at constant pressure on the plateau.

Hysteresis is the pressure difference between absorption and desorption. It differs from alloy to alloy and its origin is not fully understood.[40]

When hydrogen is absorbed by an alloy, the hydrogen molecules are dissociated into atoms upon impact with the surface.[41] Simultaneously, a solid solution is formed with an equilibrium pressure which corresponds to the hydrogen concentration. When the solution limit is reached, a new phase arises with the formation of a pressure level. When the whole alloy has transformed into this initial hydride phase, the pressure increases intensively again. The final point of the pressure level results in the stoichiometric phase. If a second hydride phase exists, another pressure level arises. With no more levels, the pressure level rises steeply. This is how we get the Pressure-Concentration isotherms. By plotting the dissociation pressures as a function of temperature, we also obtain Van't Hoff isochores and the enthalpy of formation (ΔH_f) of the system.

In the following sections, we present isotherms for several AB_5 compounds. In most cases, both absorption and desorption isotherms are shown. We have also shown the effect of deuterium in one alloy and the effect of using a mixed hydride.

$CeNi_5$ Alloy

The literature is meager on the properties of $CeNi_5$ hydrides, and its use has been ignored due to its large hysteresis during hydrogenation-dehydrogenation cycles, larger than most hydrogen-absorbing systems. However, in our search for suitable hydrides, we wished to make use of the desorption isotherm only, once the system was charged. $CeNi_5$ gives us a high hydrogen loading, a high plateau pressure and a potential for high dissociation pressure at low temperatures. In Figs. 10 and 11, we show the sorption isotherms for $CeNi_5$. In Fig. 10, the discrepancy in the +21.5°C H_2 desorption isotherm may have been caused by failure to evacuate all the deuterium used in determining a deuterium isotherm. The absorption isotherm has a plateau at 400 atm and a desorption plateau at about 60 atm (pressure difference = 340 atm). The $CeNi_5$ can be loaded to an $H/CeNi_5$ ratio of 7 at 550 atm and 21 to 22°C. At a low temperature (e.g. −21.5°C), the plateaus for absorption and desorption are 190 to 19.5 atm, respectively. The Van't Hoff plot is given in Fig. 12. Note the short plateau in Fig. 11 at −21.5°C at low H_2 loading. This indicates a phase not noted at room temperature.

It is claimed that the markedly large hysteresis is due to change in the valency of the cerium ion.[42] Lundin and Lynch have suggested that the 4+ character (vs 3+) of the ion is actually enhanced in the absorption mode and reduced in the desorption mode.[40] Cerium ions are well-known for their ability to assume 3+ or 4+ valency states.

A Moly Corporation Overview showed a Van't Hoff plot using four data points from four different sources.[43] The dissociation pressure at about −23°C is about 20 atm, well above that available with other alloys, and it compares well with our value of 19.5 atm at −21.5°C.

The $CeNi_5$ alloy was also studied for particle-size characteristics after ball-milling and after several cycles of hydriding-dehydriding. A photograph of $CeNi_5$ dehydrided powder is shown in Fig. 13. The powder particles are irregular in shape and flat. Particle-size curves of various

* Ca evaporation can also occur during homogenization, and so changes in composition can result.

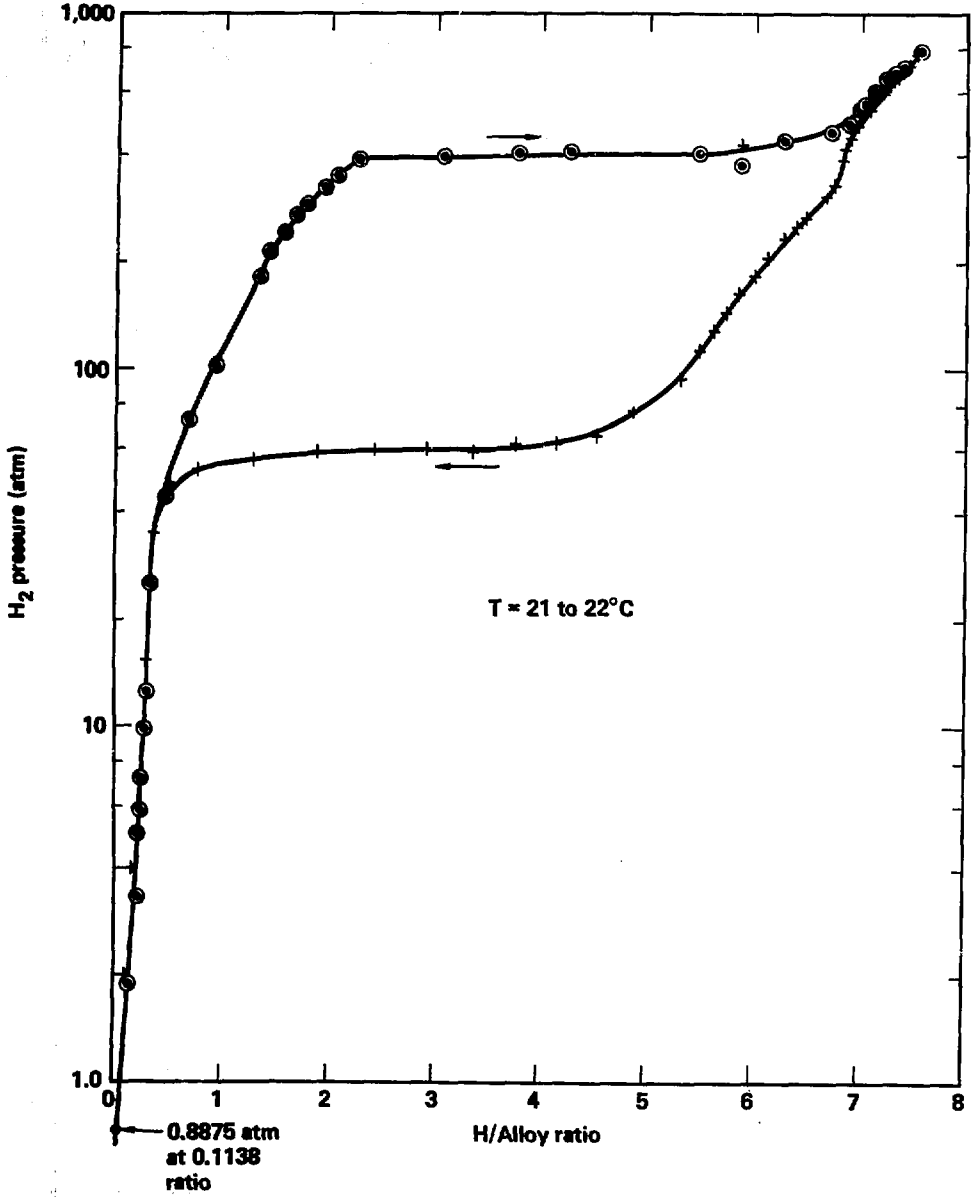

Figure 10. Static absorption-desorption isotherms for $CeNi_5H_x$ from 21 to 22°C.

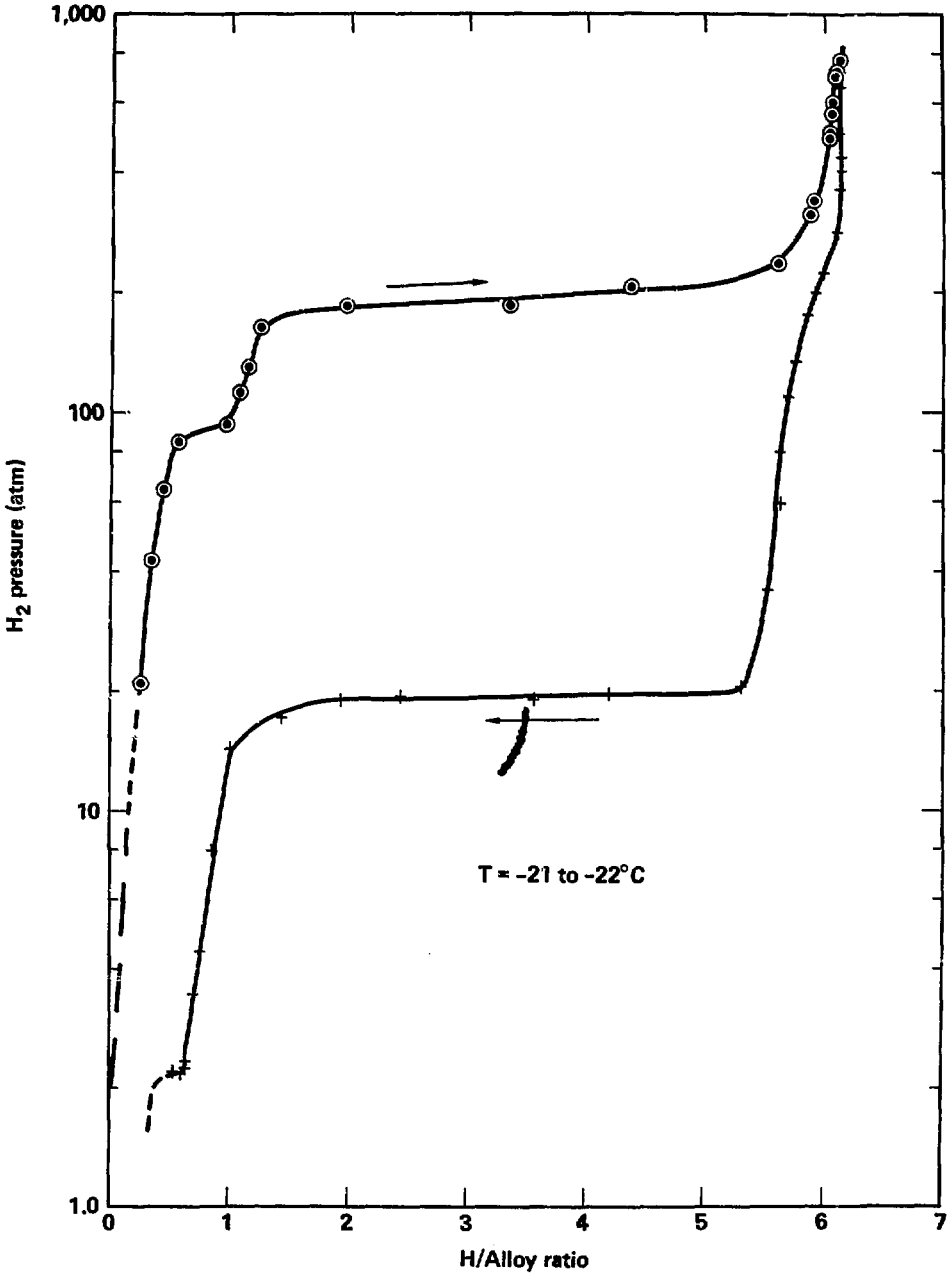

Figure 11. Static absorption-desorption isotherms for $CeNi_5H_x$ from −21 to −22°C.

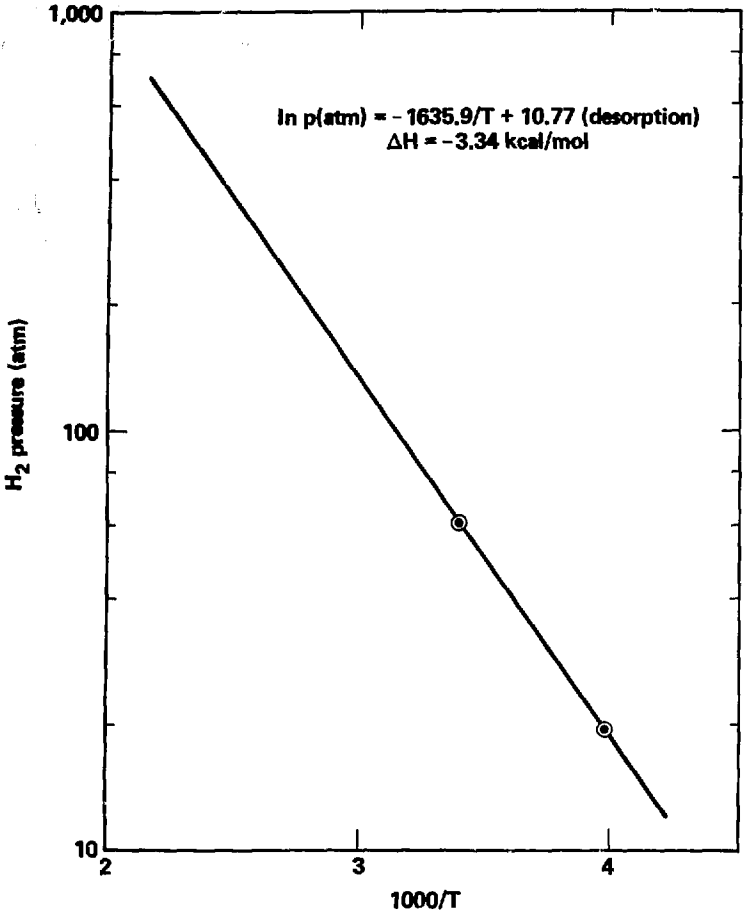

Figure 12. Van't Hoff plot for $CeNi_5H_x$.

treatments for all alloys are shown in separate sections after the isotherm portion. Bulk densities after size reduction treatment were about 4.5 g/cc.

In Fig. 14, we show the sorption isotherms of $CeNi_5$-D_2 at 22°C. The absorption isotherm increased by 100 atm and the desorption isotherm was 10 atm lower than that for hydrogen, contrary to the usual behavior for H_2-D_2 isotherms, i.e., if the deuterium isotherm is above the hydrogen absorption isotherm, then the desorption isotherm will be located above the hydrogen desorption isotherm. This discrepancy is not fully understood. The loadings are essentially the same for the two isotopes. We feel that the descending portion of the hydrogen desorption curve should follow more closely the slope of the deuterium desorption isotherm, i.e., parallel it.

The deuterium isotherms were produced to get the behavior of the deuteride were it to be used in powder transfer studies. Deuterium, being denser than hydrogen, would suspend hydride particles slightly better than hydrogen.

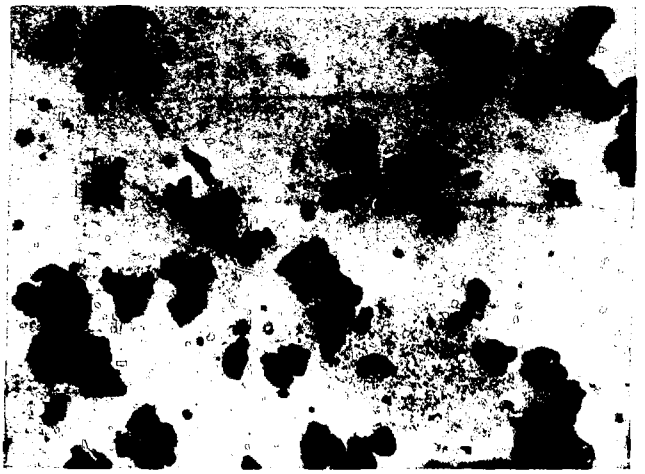

Figure 13. Batch T-83583 of $CeNi_5$ dehydrided powder. Note that the particles are flat and irregular.

$Ca_{0.2}Ce_{0.8}Ni_5$

By substituting calcium for a part of cerium, the plateau pressure and the hysteresis in $CeNi_5$ can be lowered without significantly reducing the hydrogen capacity. This composition was selected to still give a high plateau pressure (200 atm on absorption and about 22 atm on desorption). The alloy can be activated at room temperatures which was not the case with pure $CeNi_5$. The isotherms in Fig. 15 were for the alloy of the composition listed in Table 1. Compared to $CeNi_5$, the dissociation pressure of $Ca_{0.2}Ce_{0.8}Ni_5$ would be less. These isotherms were obtained on the first cycle on material crushed to a 2–3 mm mean diameter.

$Ca_{0.2}Mm_{0.8}Ni_5$

$CaNi_5$ and $MmNi_5$ are soluble over a complete range. By substituting the cerium with calcium, the plateau pressures and hysteresis are lowered over that found in pure mischmetal nickel alone. The Ca_x-Mm_{1-x}-Ni_5 system offers the advantages of low raw material cost and easy activation. The plateau pressures may be tailored for pressure without sacrificing capacity. The hydrogen capacity is not reduced substantially. The desorption plateau pressure 35 atm at midpoint, is approximately 17 atm greater than that of $Ca_{0.2}Ce_{0.8}Ni_5$ (Fig. 16). However, this alloy has the added advantage that when high temperatures are encountered, the dissociation pressures will not be as great as in the $CeNi_5$ hydride. The composition cited above is a nominal composition; it was actually $Ca_{0.167}Mm_{0.7884}Fe_{0.0517}Ni_5$.

In alloys containing mischmetal, hysteresis and plateau pressures are affected by the Ce/La ratio of the mischmetal obtained and by the source of Mm. Mischmetal obtained from bastinite ores contains 50% cerium while that mined from monazite contains 65% cerium.

The dissociation pressure for a $Ca_{0.2}Mm_{0.8}Ni_5$ alloy at −20°C is reported by Ergenics to be 5 atm extrapolated from a Van't Hoff plot. The equation is—

$$\ln P(\text{atm}) = \frac{-2923}{T} + 13.08 \quad .^{44} \qquad (1)$$

Here again, the plateaus are not flat and are reportedly due to segregation effects, especially calcium and mischmetal—rare earths and calcium have little affinity for each other.[45]

$Ca_{0.2}(Ce_{0.65}Mm_{0.35})_{0.8}Ni_5$

This alloy is a modification of the alloy $Ca_{0.2}Mm_{0.8}Ni_5$. The amount of total cerium has been increased. Mischmetal already contains cerium. The sorption isotherms at 22°C are shown in Fig. 17. The major effect has been to increase the hysteresis. We have gained some additional hydrogen capacity at a slight reduction in the desorption isotherm. The gain is about one unit in the H/alloy ratio.

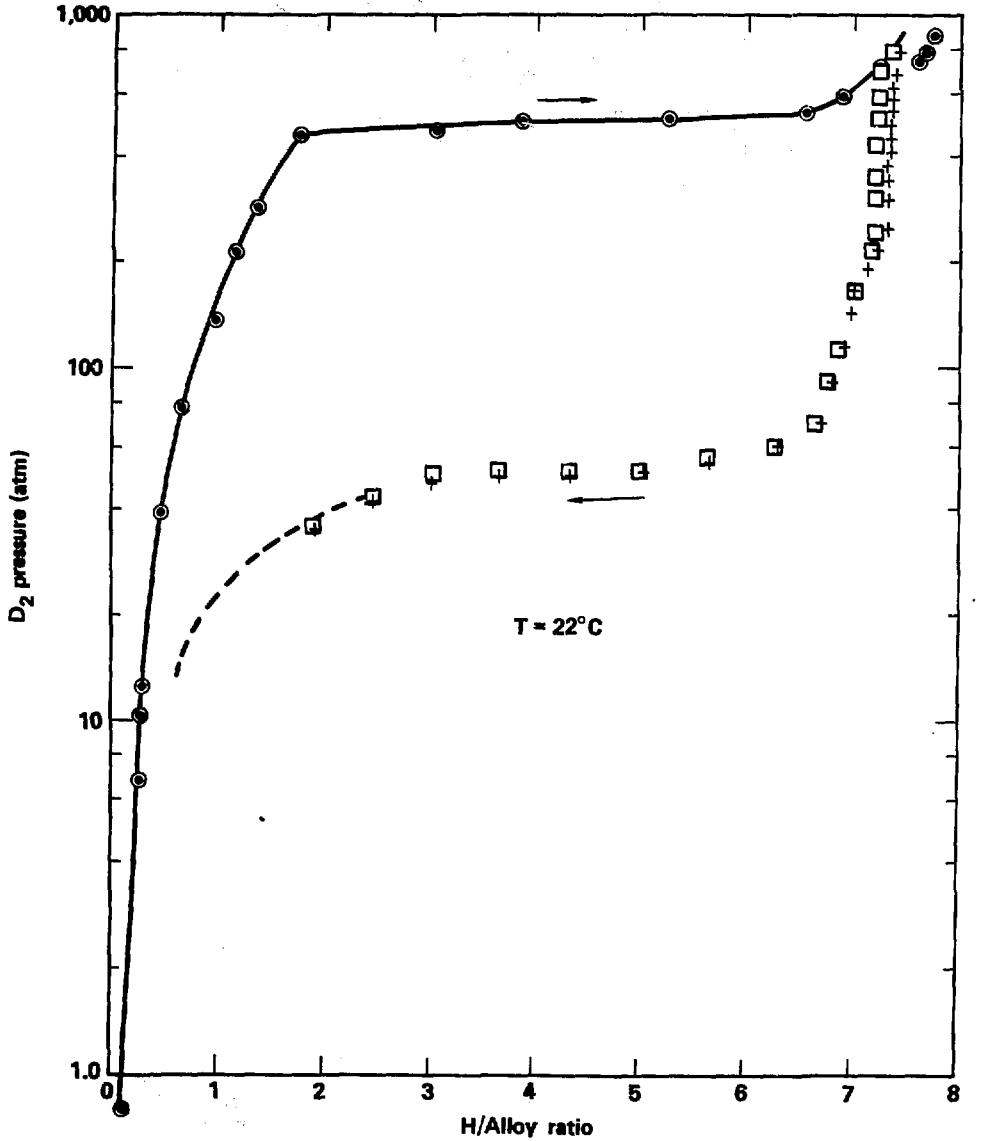

Figure 14. Static absorption-desorption isotherms for CeNi-D_2 at 22°C.

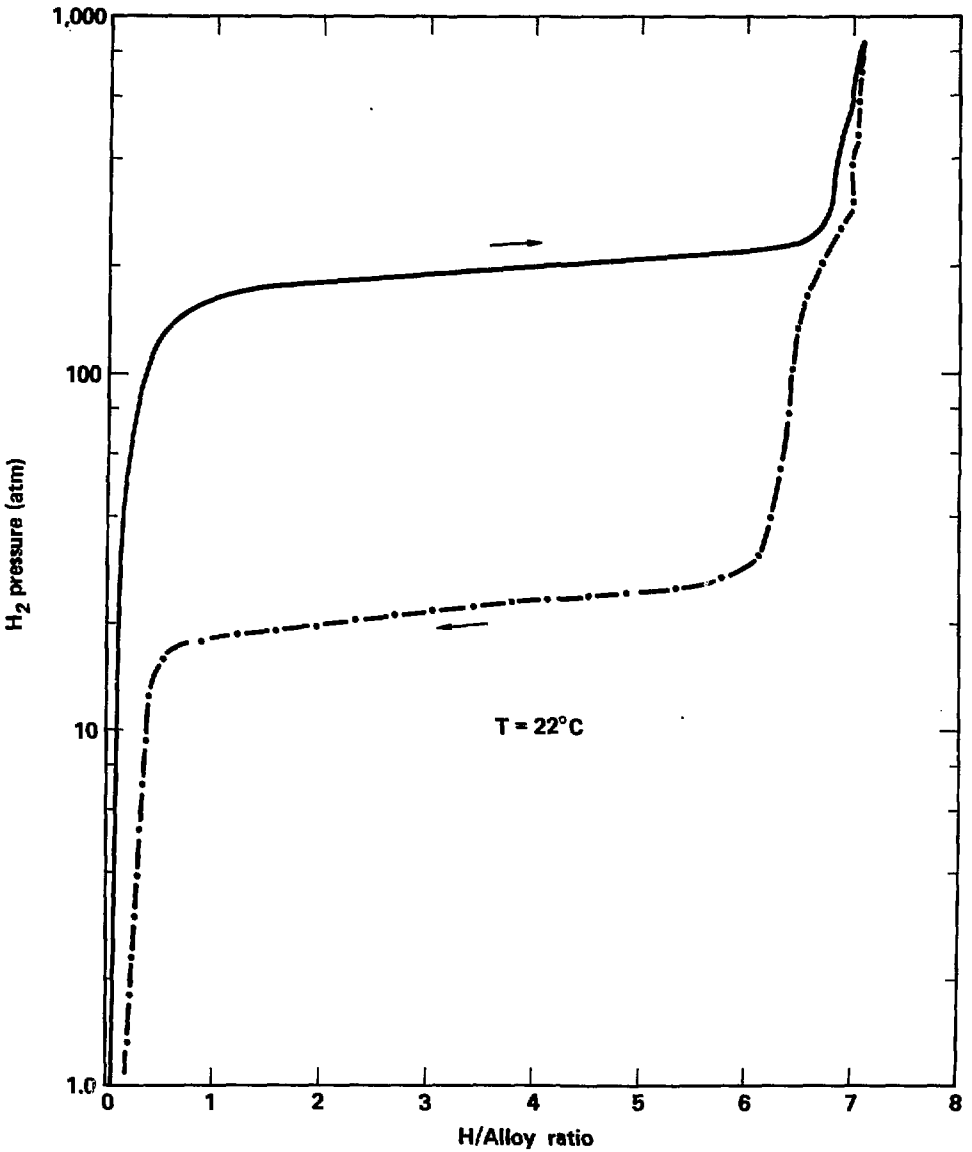

Figure 15. Static absorption-desorption isotherms for $Ca_{0.2}Ce_{0.8}Ni_5$ at 22°C (first cycle—no activation).

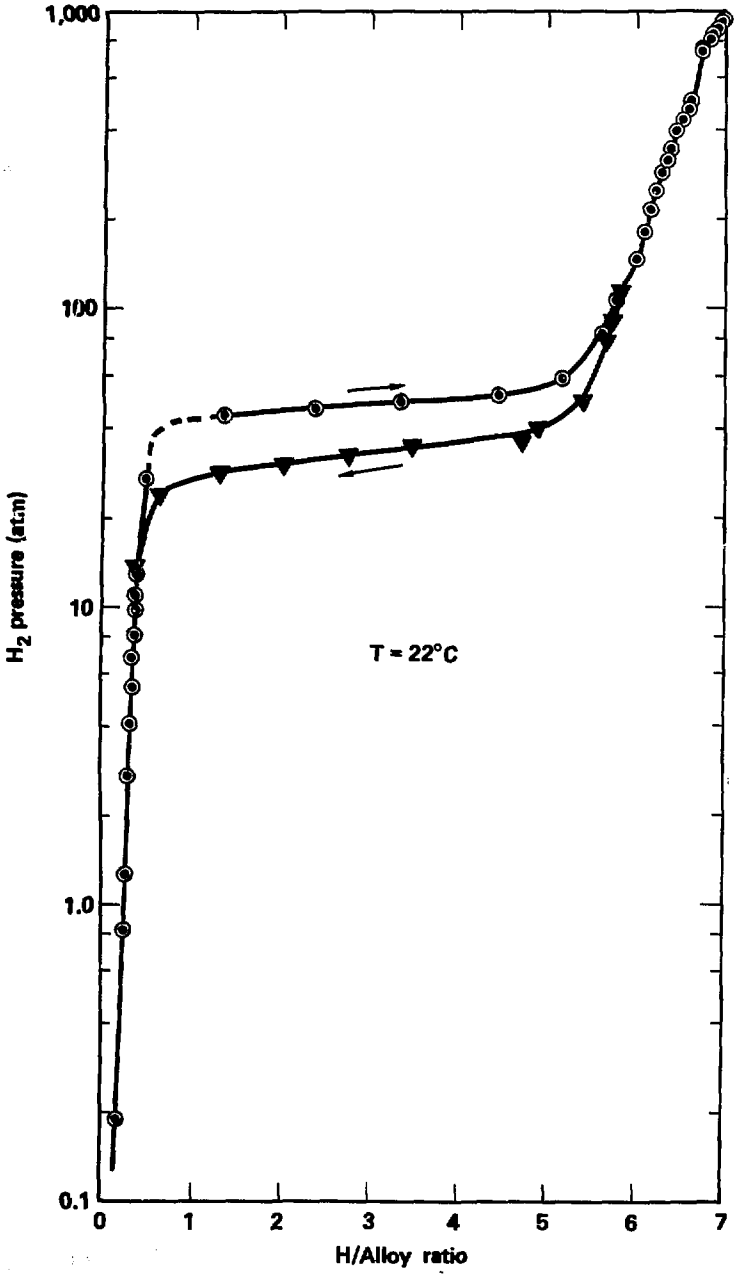

Figure 16. Static absorption-desorption isotherms for $Ca_{0.167}Mm_{0.7984}Fe_{0.517}Ni_5$ at 22°C (Hystor 203, Batch T-84159).

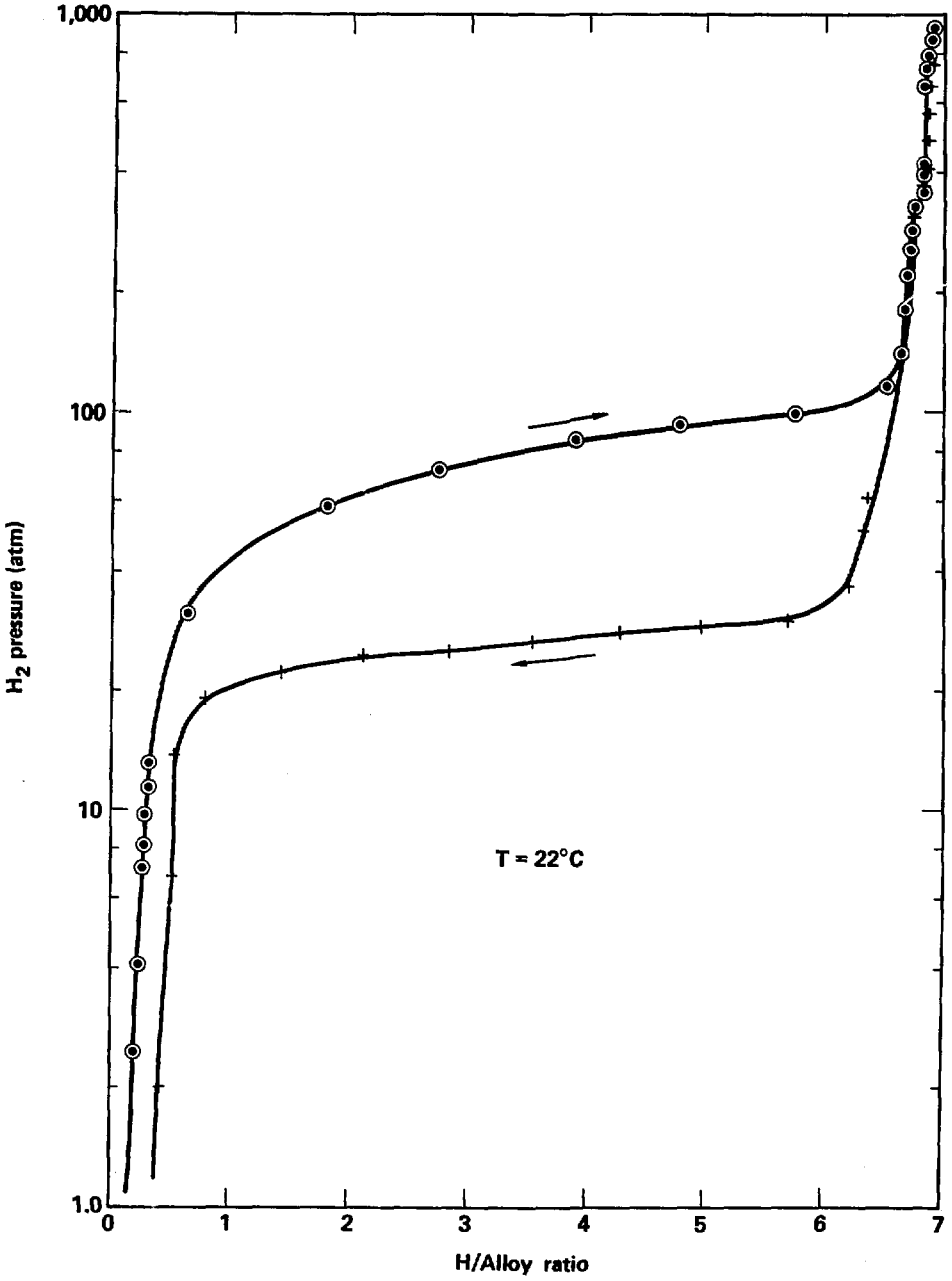

Figure 17. Static adsorption-desorption isotherms for $Ca_{0.2}(Ce_{0.65}Mm_{0.35})_{0.8}Ni_5H_x$ at 22°C.

Mixed Hydrides $CeNi_5/MmNi_5$

There have been very few investigations in developing isotherms for two different types of hydrides. Suda and Uchida reported working on mixtures of $LaNi_5$ + TiFe and $LaNi_5$ + $Ti_{0.8}Zr_{0.2}Cr_{0.8}Mm_{1.2}$.[46] Lowering the pressure at maximum hydrogen capacity is useful when working at high temperatures. We used one mixture to determine how the Pressure-Concentration isotherm diagram could be modified.

We used a 50:50 mix of $CeNi_5$ and $MmNi_5$ alloy with the $CeNi_5$ being previously activated at low temperatures and at a 10-kpsi hydrogen gas pressure. Figure 18 shows the absorption isotherm of the 50:50 mixed together with those for $MmNi_5$ and $CeNi_5$. Figure 19 shows the desorption isotherms for the three alloys. The $MmNi_5$ isotherms were plotted from Ref. 28, but high pressure data

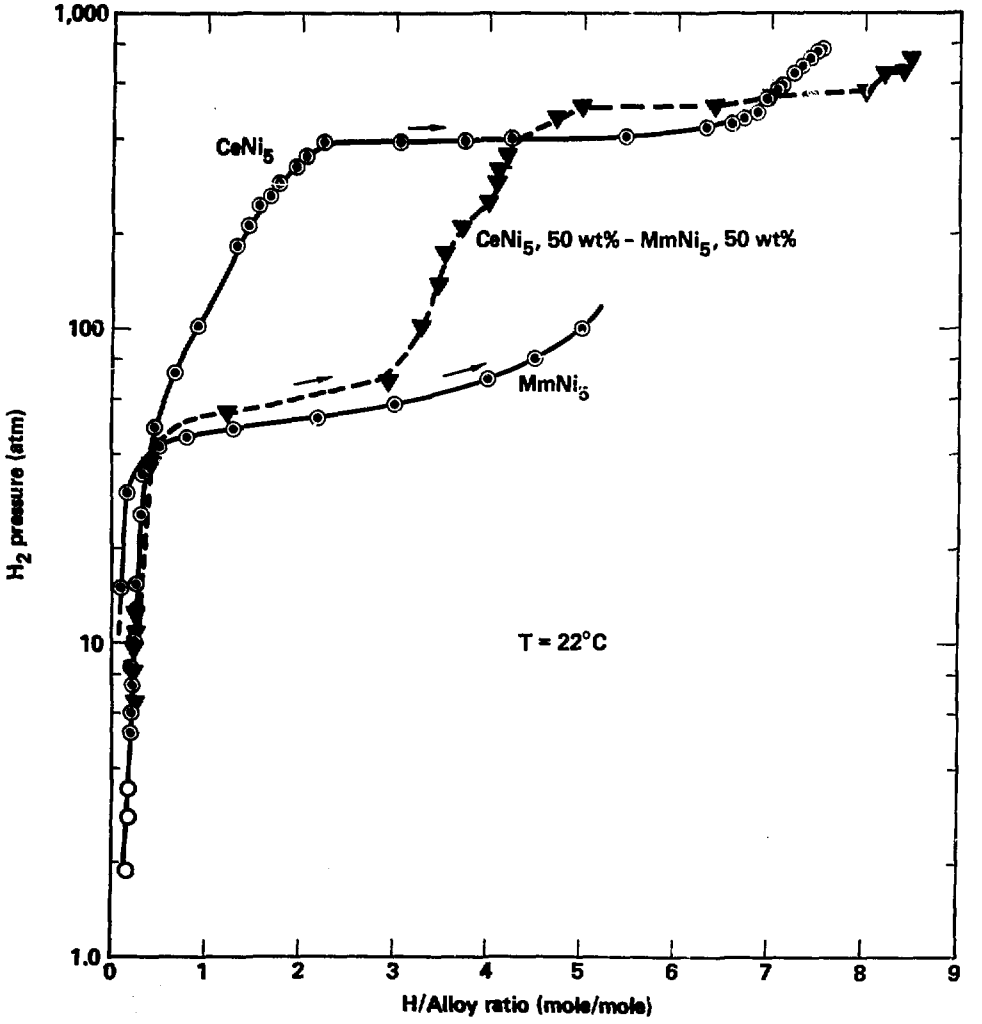

Figure 18. Static adsorption isotherm for a mixed hydride ($CeNi-MmNi_5$) at 22°C.

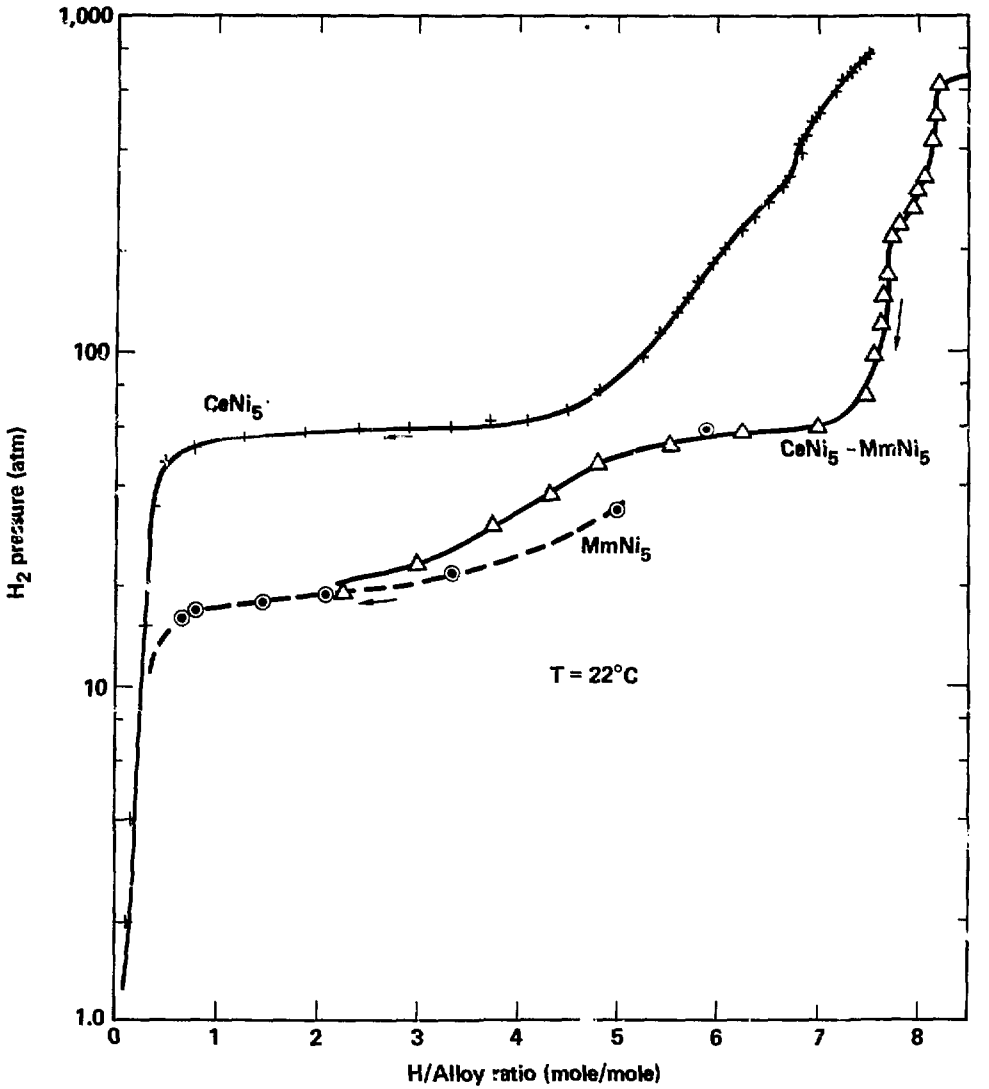

Figure 19. Static desorption isotherm for a mixed hydride ($CeNi_5$-$MmNi_5$) at 22°C.

were not available. Note that combined isotherm in Fig. 18 is a "step function," i.e., the initial portion of the plot behaves like the dissociation pressure counterpart and the remainder of the plot behaves like the high dissociation alloy. It is not understood why the $CeNi_5$-$MmNi_5$ absorption isotherm is greater than that of the pure $CeNi_5$ at the high hydrogen capacity end. The plot shows a high capacity (1 unit greater than pure $CeNi_5$).

Summary of Some Properties

We have summarized some properties of the hydrides investigated and these are shown in Table 3.

Table 3. Some properties of the alloys investigated.

Alloy	Plateau slope desorption dp/d (H/alloy)	Capacity for H_2, D_2 H/alloy (end of plateau)	Plateau pressures at mid-pt (atm) at 21.5°C		Plateau pressures at mid-pt (atm) at −21.5°C	
			absorb	desorb	absorb	desorb
$CeNi_5$	2	7 (H_2)	390	~60	190	19.5
	0	7 (D_2)	500	~51		
$Ca_{0.2}Ce_{0.8}Ni_5$	1	~6.5	190	22		
$Ca_{0.2}Mm_{0.8}Ni_5$	3	~5.5	48	33		
$Ca_{0.2}(Ce_{0.65}Mm_{0.35})_{0.8}Ni_5$	1.7	~6	74	~26		
$CeNi_5/MmNi_5$ 50:50 wt%	13	~7 from desorption curve	2 plateaus			
$MmNi_5$[a]	6.7	(?)	~58	20		

[a] Ref. 28.

Particle-Size Characterization

The following section contains particle-size distribution curves for the alloy investigated. Curves are for one hydriding-dehydriding cycle.

Particle-Size Distribution After Initial Isotherm

Particle-size distributions of the intermetallic alloys were determined after the first absorption-desorption cycle by means of the Quantamet analyzer. The plot of the weight percent below size vs the diameter in microns is shown in Figs. 20–24. These are the standard "S" or ogive curves. Table 4 is a tabulation of the particle size at the 50 wt% less than size point.

Table 4. Maximum particle size in the lower 50 wt% portion of six hydrides and maximum size after first hydriding-dehydriding cycle.

Alloy	Size at 50 wt% (μ)	Maximum size (μ)
$CeNi_5$	21, 41	60
$Ca_{0.2}Ce_{0.8}Ni_5$	9.5	32
$Ca_{0.2}Mm_{0.8}Ni_5$	25, 33	58, 94
$Ca_{0.2}(Ce_{0.65}Mm_{0.35})_{0.8}Ni_5$	18	100
$MmNi_5$	18	65
Mixed Hydrides		

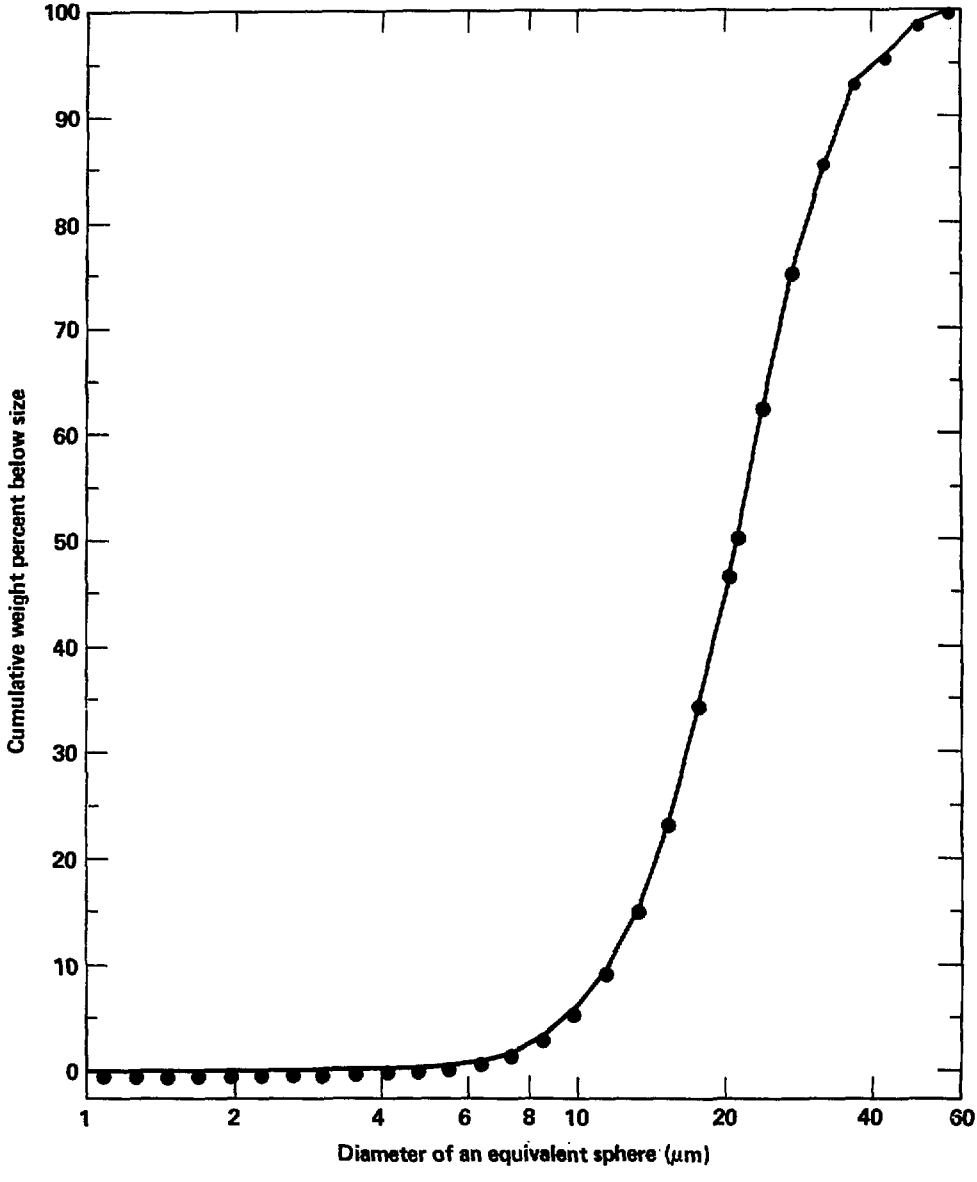

Figure 20. Particle-size distribution curve for $CeNi_5$ after the first hydriding-dehydriding cycle.

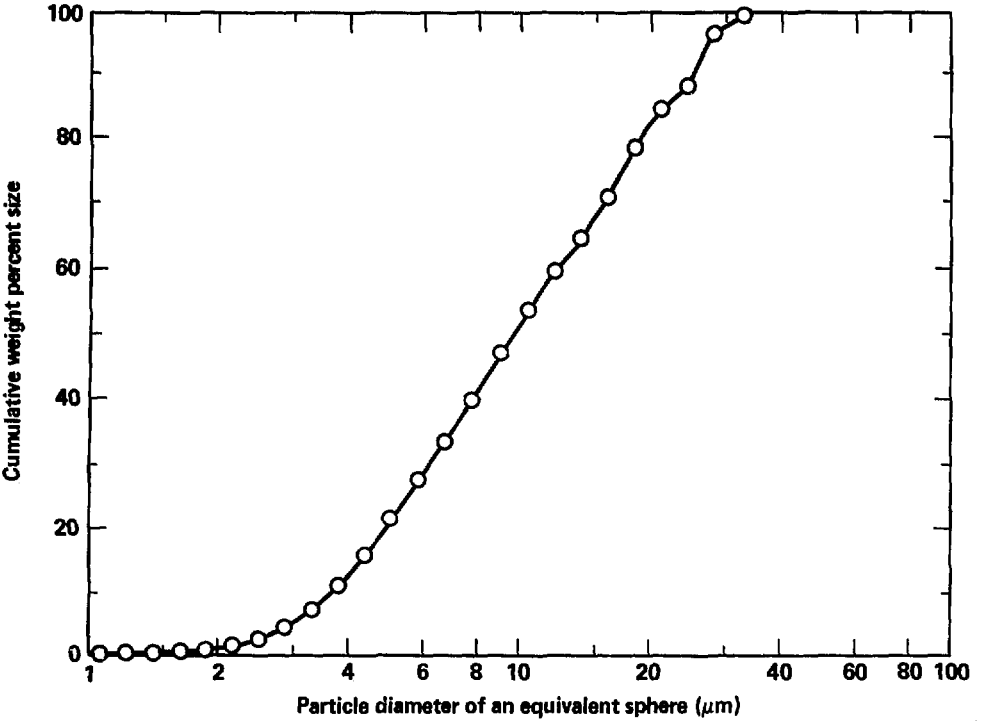

Figure 21. Particle-size distribution curve for $Ca_{0.2}Ce_{0.8}Ni_5$ which was ball-milled for 16 h, hydrided and dehydrided.

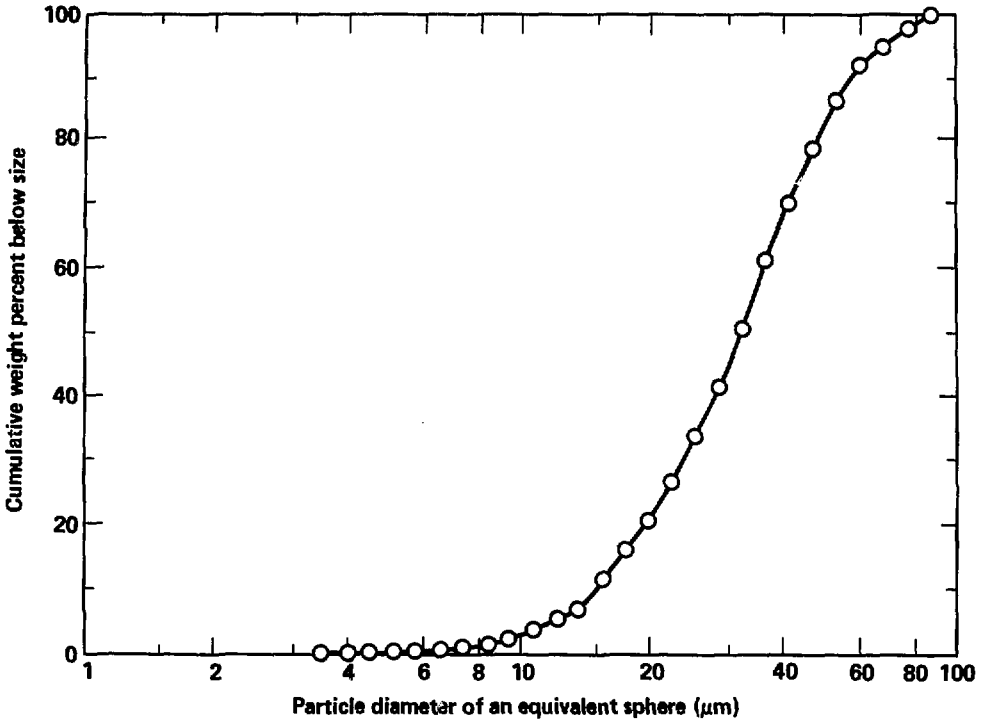

Figure 22. Particle-size distribution curve for $Ca_{0.2}Mm_{0.8}Ni_5$ which was hydrided and dehydrided.

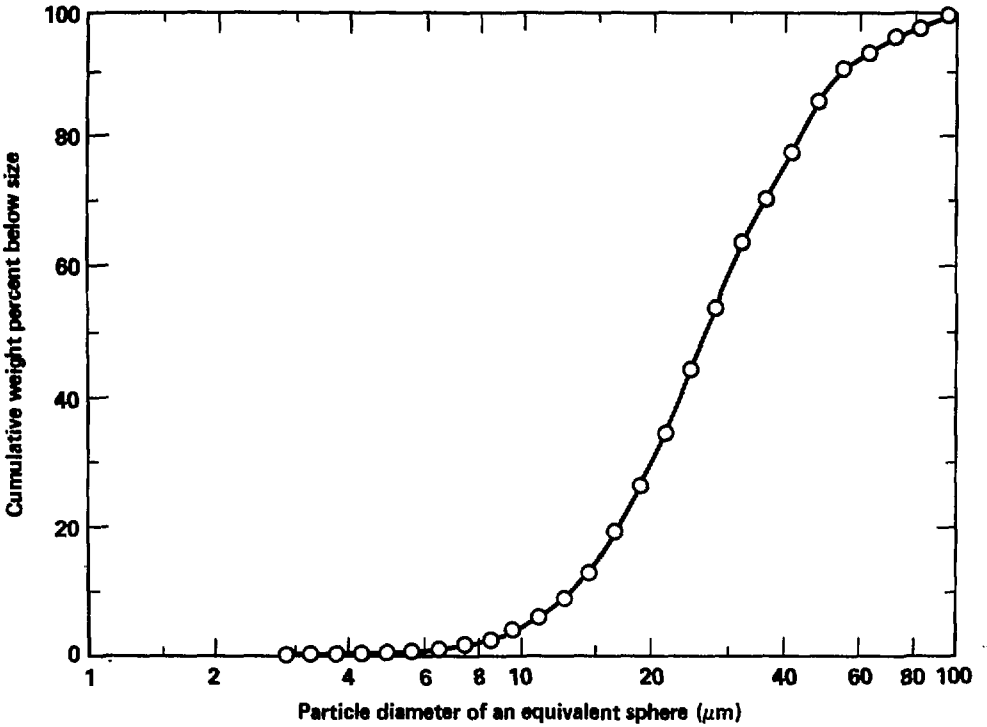

Figure 23. Particle-size distribution curve for $Ca_{0.2}(Ce_{0.65}Mm_{0.35})_{0.8}Ni_5$ which was hydrided and dehydrided.

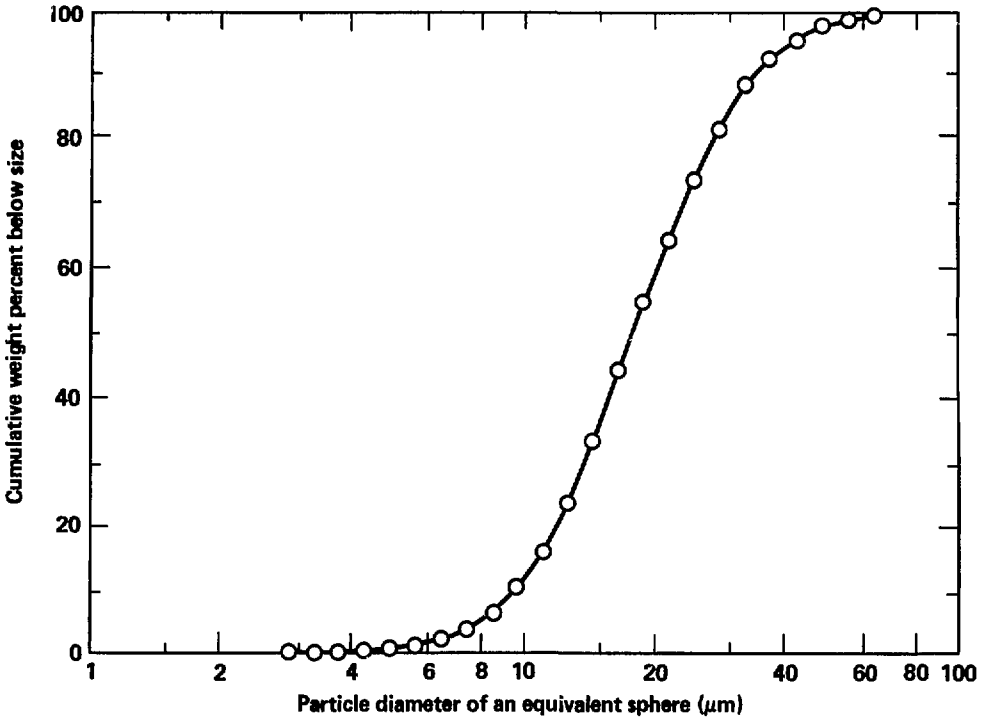

Figure 24. Particle-size distribution curve for $MmNi_5$ which was hydrided and dehydrided.

This section contains particle-size distribution curves for $CeNi_5$ hydrided-dehydrided 1–12 cycles.

Particle-Size Distribution After Repeated Cycling with Hydrogen

After activating the $CeNi_5$, we wished to determine the reduction in particle size upon subsequent hydriding-dehydriding cycles to determine whether there was a minimum diameter. Fine particles were desired for transfer experiments. We subjected $CeNi_5$ to 12 cycles and after each cycle sampled the dehydrided material. The results are shown in Figs. 25–29 and in Table 5.

The small discrepancy between cycles 9 and 12 is probably due to sampling and clustering of particles. In order to make a reasonable analysis, we put the $CeNi_5$ through 325- and 400-mesh screens prior to sampling. This procedure also eliminated any trash which came in from the original melt. Apparently, the break point is somewhere in the vicinity of 15 cycles.

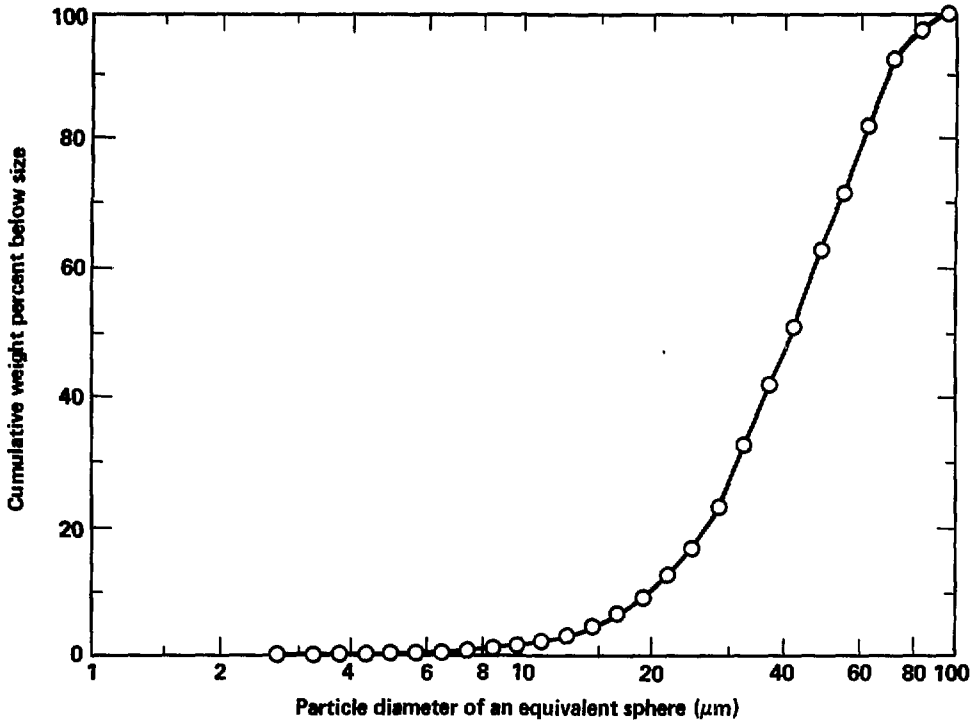

Figure 25. Particle-size distribution curve for $CeNi_5$, hydrided and dehydrided, at end of first cycle.

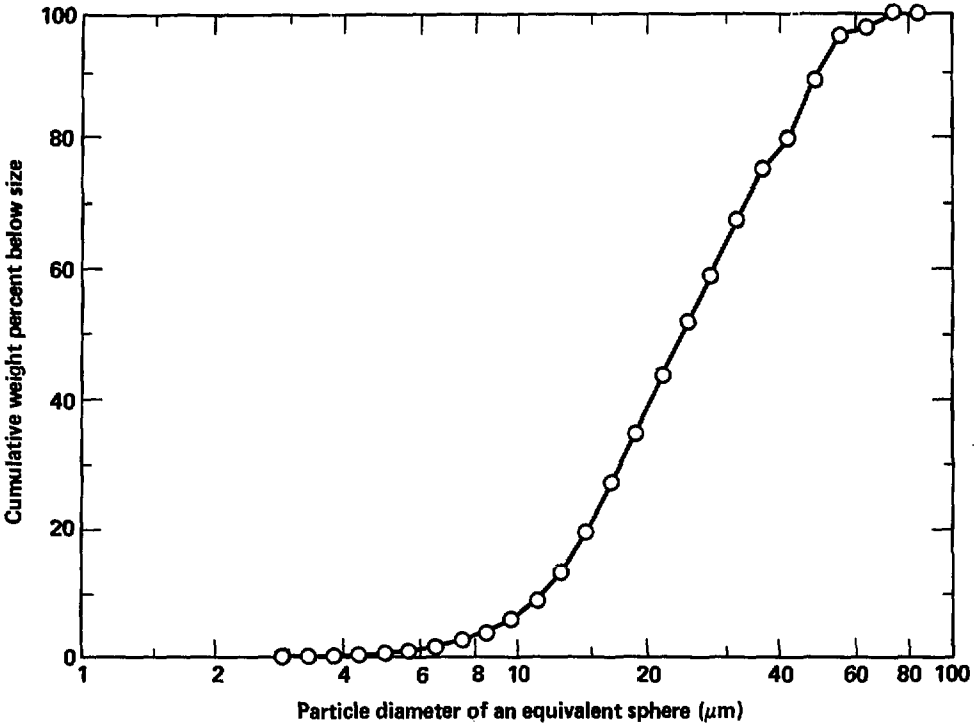

Figure 26. Particle-size distribution curve for $CeNi_5$, hydrided and dehydrided, at end of second cycle, using material from first cycle.

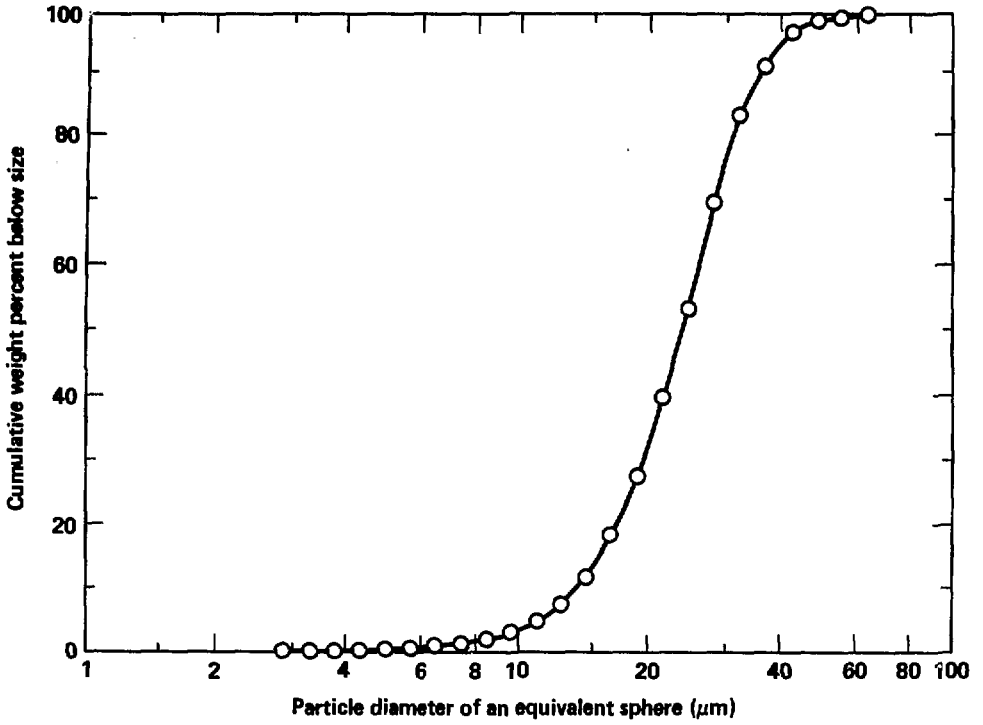

Figure 27. Particle-size distribution curve for $CeNi_5$, hydrided and dehydrided, at end of third cycle, using material from second cycle.

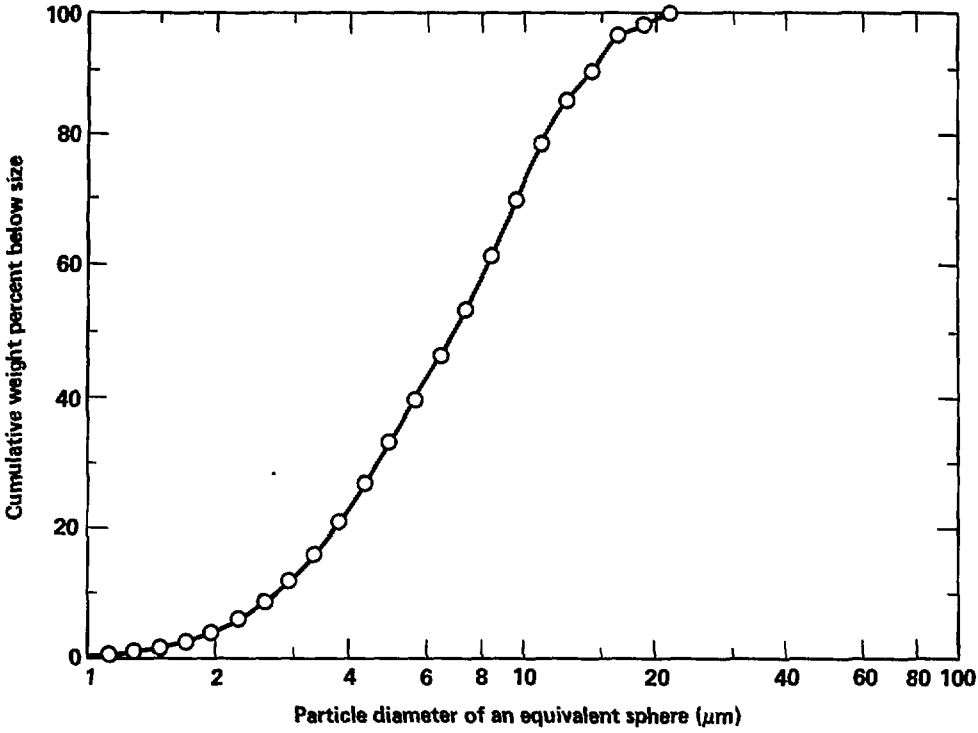

Figure 28. Particle-size distribution curve for $CeNi_5$, after nine cycles of hydriding and dehydriding. This was a sample separate from that used in Figs. 25, 26 and 27.

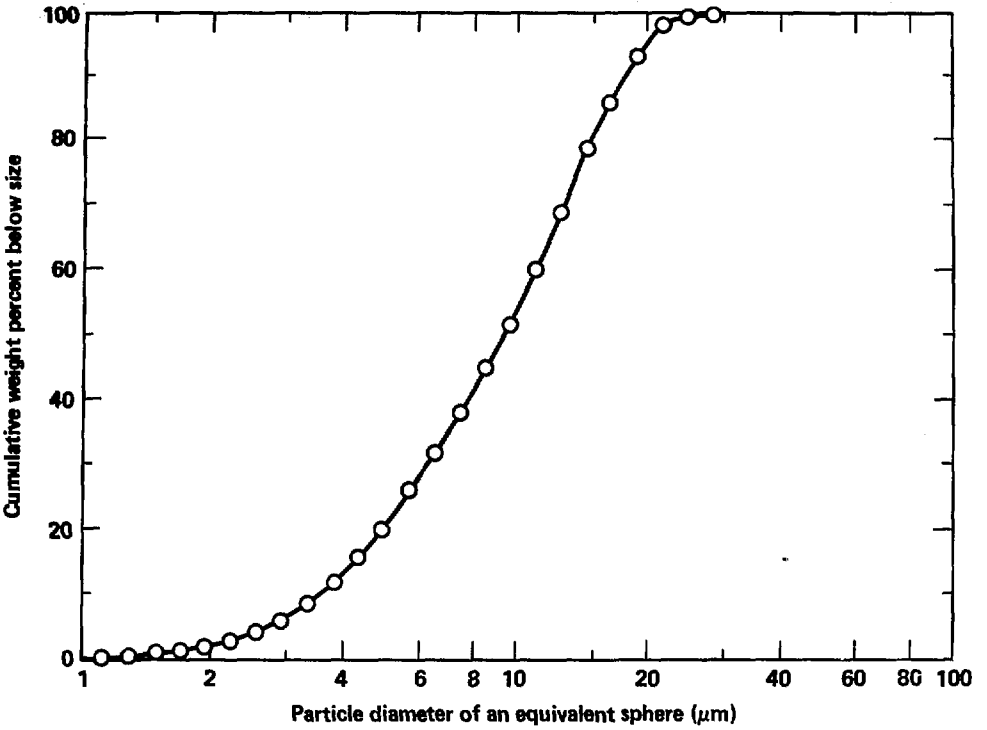

Figure 29. Particle-size distribution curve for $CeNi_5$, after twelve cycles of hydriding and dehydriding. The sample from Fig. 28 was used.

Table 5. Maximum particle size in the lower 50 wt% portion of $CeNi_5$ and maximum size after several cycles of hydriding.

Alloy	Size at 50 wt% (μ)		Maximum size (μ)
$CeNi_5$ cycle 1	41	See curve for variation in "S" curve	100
$CeNi_5$ cycle 2	23		85
$CeNi_5$ cycle 3	23		65
$CeNi_5$ cycle 9	7		22
$CeNi_5$ cycle 12	9.7		30

This section contains particle-size distribution curves for $CeNi_5$ ball-milled for various length of times.

$CeNi_5$ Ball-Milled

The as cast $CeNi_5$ was broken into 2–5 mm mean diameter pieces, and ground in a ball mill for 8 and 16 hours; the 16-hour sample was hydrided and dehydrided. The particle-size distribution curves are shown in Figs. 30–32 and a summary is shown in Table 6.

From this data, it appears that ball-milling to achieve the desired particle size for hydride transfer is the more rapid method.

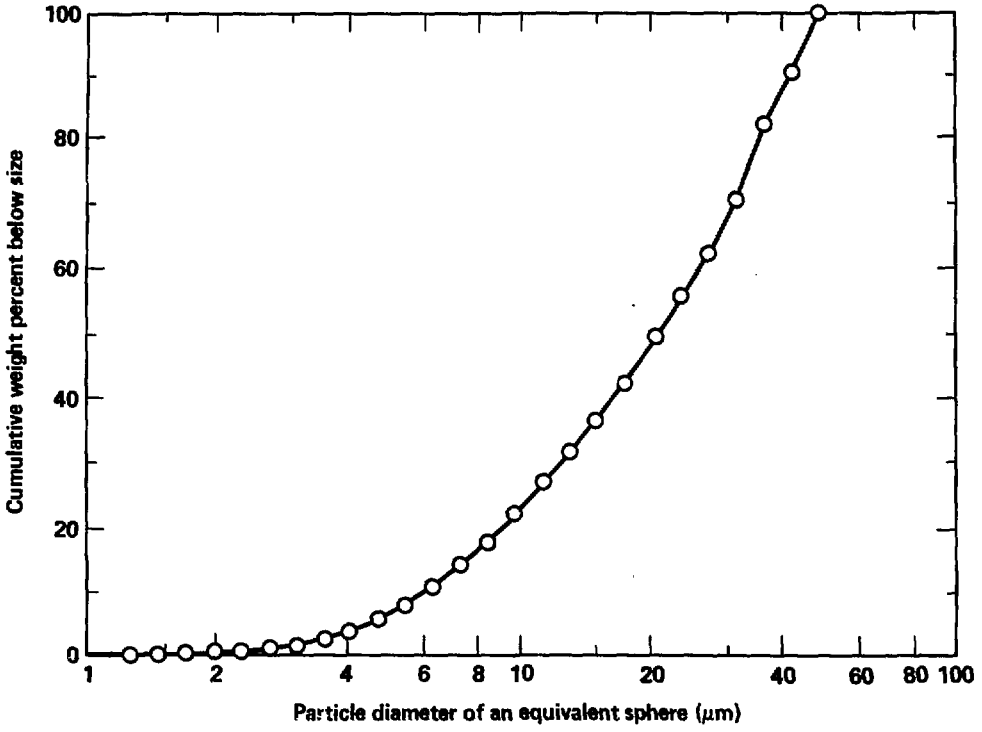

Figure 30. Particle-size distribution curve for $CeNi_5$ which was ball-milled for 8 h.

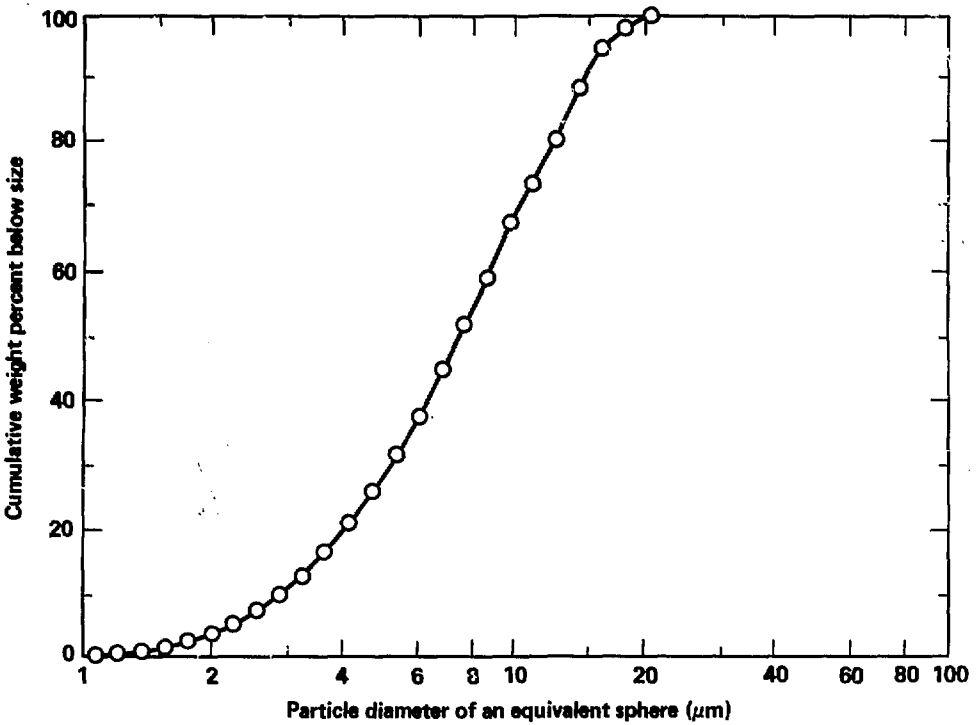

Figure 31. Particle-size distribution curve for $CeNi_5$ which was ball-milled for 16 h.

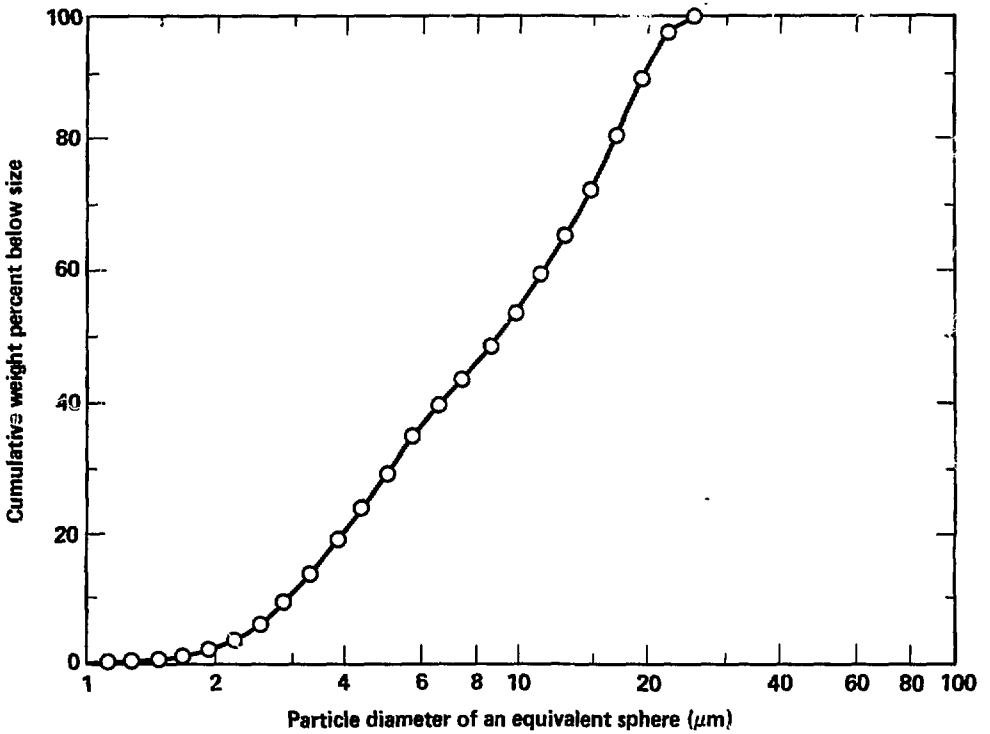

Figure 32. Particle-size distribution curve for $CeNi_5$ which was ball-milled for 16 h, hydrided and dehydrided.

Table 6. Particle-size analysis results for $CeNi_5$ after ball-milling.

Alloy	Time in ball mill (h)	Size at 50 wt% less than size point (μ)	Maximum size (μ)
$CeNi_5$	8	20	50
	16	7.2	21
	16, Hydrided and Dehydrided	8.5	25, 30

Powder Transfer

The objective of this portion of our study was to gain a better understanding of the behavior of the metal hydride undergoing a gaseous transport process, which consists of storing the metal in the form of a very fine powder in equilibrium with the high-pressure hydrogen gas and then allowing the solid-gas mixture to expand freely into an initially evacuated vessel. The powder is fluidized and transported by the energy of the expanding gas. Most of the alloys are brittle by nature and can be reduced to fine powders of the size of a few microns, thus making transport by gas feasible.

Parameter Considerations

This was a study of fluid mechanics of the solid-gas, two-phase system with the variables being metal powder loading, gas-to-metal mole ratio for a given geometry, storage pressure, storage reservoir-to-receiving reservoir volume ratio, storage temperature, particle size (distribution), and type of alloy with its distinctive absorption-desorption characteristics. The gas-to-solid loading ratios (in mole/mole), α, as a function of the metal loading, are calculated and plotted in Fig. 33 for various storage volumes of 60, 120, 160 and 250 cc. The solid (powder) occupies only a fraction of the storage volume. The solid storage-to-single-phase storage ratio, β, for various storage volumes, is a linear function of the metal loading and is also shown in Fig. 33. This is an indication of the effectiveness of the solid storage scheme using the metal hydride. The metal used was $CeNi_5$ with a saturation hydrogen composition of 6.75 H/Metal ratio. The single-phase storage is the amount of gaseous hydrogen in moles occupying the same volume under the same pressure. For a given storage volume (V_1), the gas-to-metal loading ratio, α, decreases parabolically and the solid storage-to-single-phase storage ratio, β, increases linearly with increasing metal hydride loading. Since the fluid mechanics of the gas-solid flow calls for an adequate level of α to achieve any degree of success with the metal powder transfer, the storage ratio would have to be sacrificed. The values may have to be in the 1.5 to 3.0 range, much lower than the theoretical values of 5.6 which is achievable only if the metal hydride exists as a single piece of solid metal without any gaseous free space. The hydride powder can become fluidized by the turbulent hydrogen gas that originally coexists in equilibrium with the hydride in the high-pressure storage reservoir. The fluidization and mixing actions are induced by the rapid expansion and discharge of the gas-solid mixture into the receiving reservoir and aided at the same time by the desorption process which generates most of the gas.

During a free expansion process for a pure gas system, the gas remaining in the storage reservoir is generally considered to undergo nearly reversible adiabatic expansion accompanied by a temperature drop,[47] and the gas arriving at the receiving reservoir undergoes an adiabatic compression accompanied by a temperature rise. The deviations from the reversible adiabatic process are due to irreversible processes such as fluid friction and heat transfer, even in the earliest phases of an expansion or compression. For a metal hydride powder-hydrogen system, the deviations will be greater due to higher levels of friction caused by the powder. Larger temperature drops and rises, relative to free expansion of the pure gas, are also expected because of the desorption and absorption heat exchange.

The final equilibrium pressure following the free expansion is a new point on the desorption isotherm determined by the intersection on the equation of a straight line correlating the gas pressure with the amount of gas in the gaseous space.

Results and Discussion of Powder Transfer Experiments

Table 7 summarizes the results of four transfer tests with and without the hydride powder using the 2247.5 cc or 1026.5 cc receiving reservoirs. Figure 34 compares the pressure and temperature transients, typically experienced by the gas remaining in the storage reservoir, between a metal powder transfer and a pure gas transfer. The following results are noted:

- Both powder transports into either 2247.5 cc or 1026.5 cc receivers were 100%, demonstrating the feasibility of gaseous metal powder transfer.
- The effects of metal hydride powder on the expansion cooling and compression heating during the transfer process are significant as shown in Table 7 and Fig. 34. The storage reservoir experienced larger temperature drops for the metal transfer runs (48.5°C and 50.5°C) as compared to the pure gas tests (21°C and 20.5°C), due to the additional cooling effect of (hydrogen) desorption. The receiving reservoirs, on the other hand, saw less temperature rises for the metal transfer cases, 21°C and 26°C vs 28°C and 48°C, respectively.

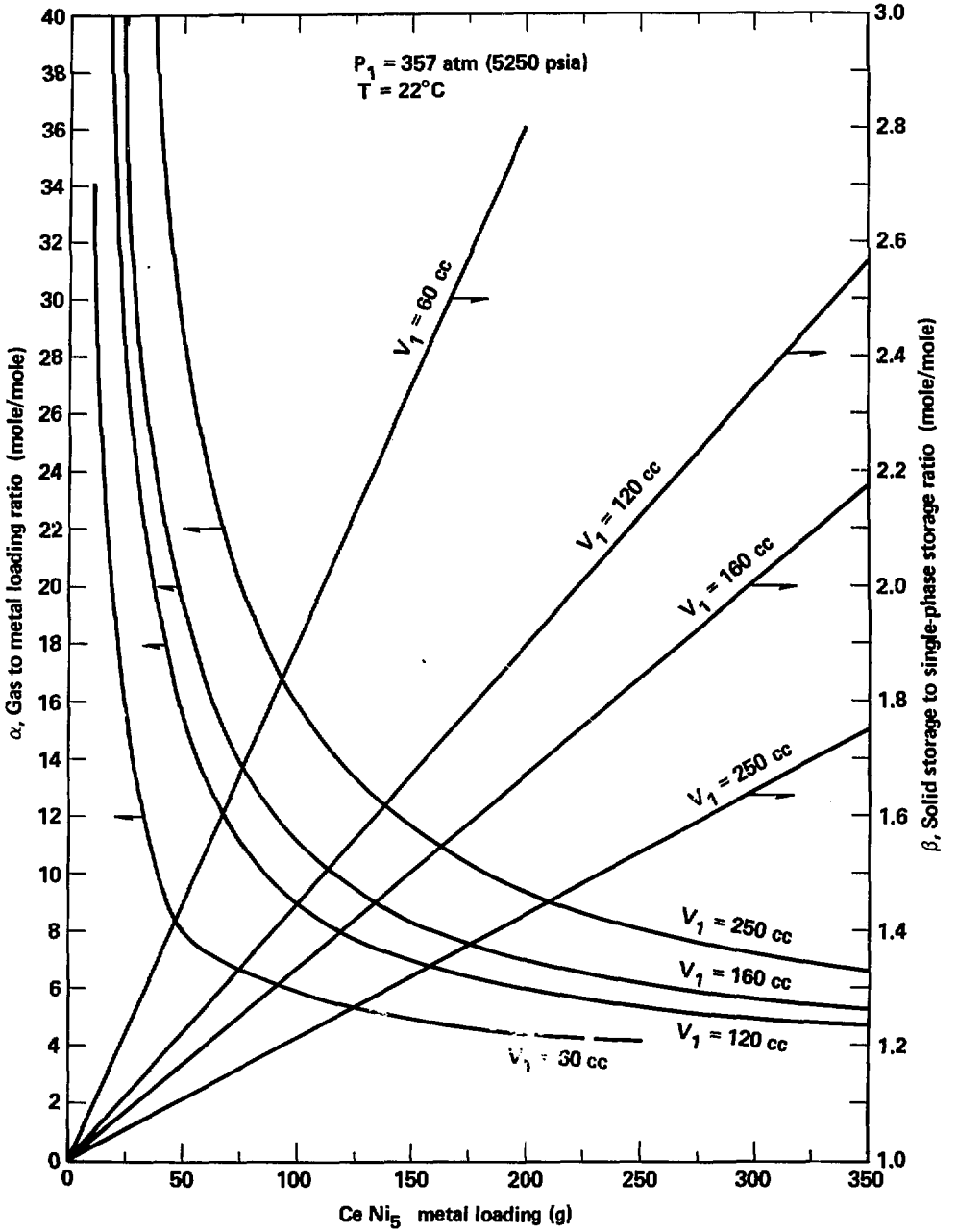

Figure 33. α, gas-to-metal loading ratio vs $CeNi_5$ metal loading.

Table 7. $CeNi_5H_x$ powder transfer data.

	Storage (160 cc)				
	x	Initial pressure (psig)	Metal loading (g)	T_{min} (°C)	Time to reach t_{min} (s)
$CeNi_5H_x$	5.86	5285.0	180.4	−25.5	2.7
$CeNi_5H_x$	~5.70	5378.0	202.0	−27.5	2.1
All Gas	–	5319.0	–	2.0	0.6
All Gas	–	5273.2	–	2.5	0.3

	Receiver			
	Size (cc)	T_{max} (α)	Time to reach T_{max} (s)	Final pressure (psig)
$CeNi_5H_x$	2247.5	44.0	2.4	293.0
$CeNi_5H_x$	1026.5	49.0	~	551.0
All Gas	2247.5	51.0	4.5	290.2
All Gas	1026.5	68.0	1.2	544.2

- The presence of metal powder slowed down the transfer time, as expected (see Fig. 34). The pressure tracing for the metal transfer in Fig. 34 shows a definite change in the slope, at the point before which the flow was in the solid-gas, two-phase region and beyond which the flow was pure gas, as evidenced by the slope being equal to that of pure gas flow curve on the left.
- The effect of the receiving reservoir volume size is negligible at least for the range tested.
- Better temperature measurements are needed so that the thermodynamic data such as ΔH, the enthalpy of hydride formation, can be deduced. This may include accurate determinations of the emissivities of thermocouple junctions (including surface conditions and materials), simultaneous measurements of the thermocouple and wall temperatures during expansions and better insulation of the test vessels.
- Other metal hydrides and different volume ratios, and metal loadings at other temperature conditions should be investigated.

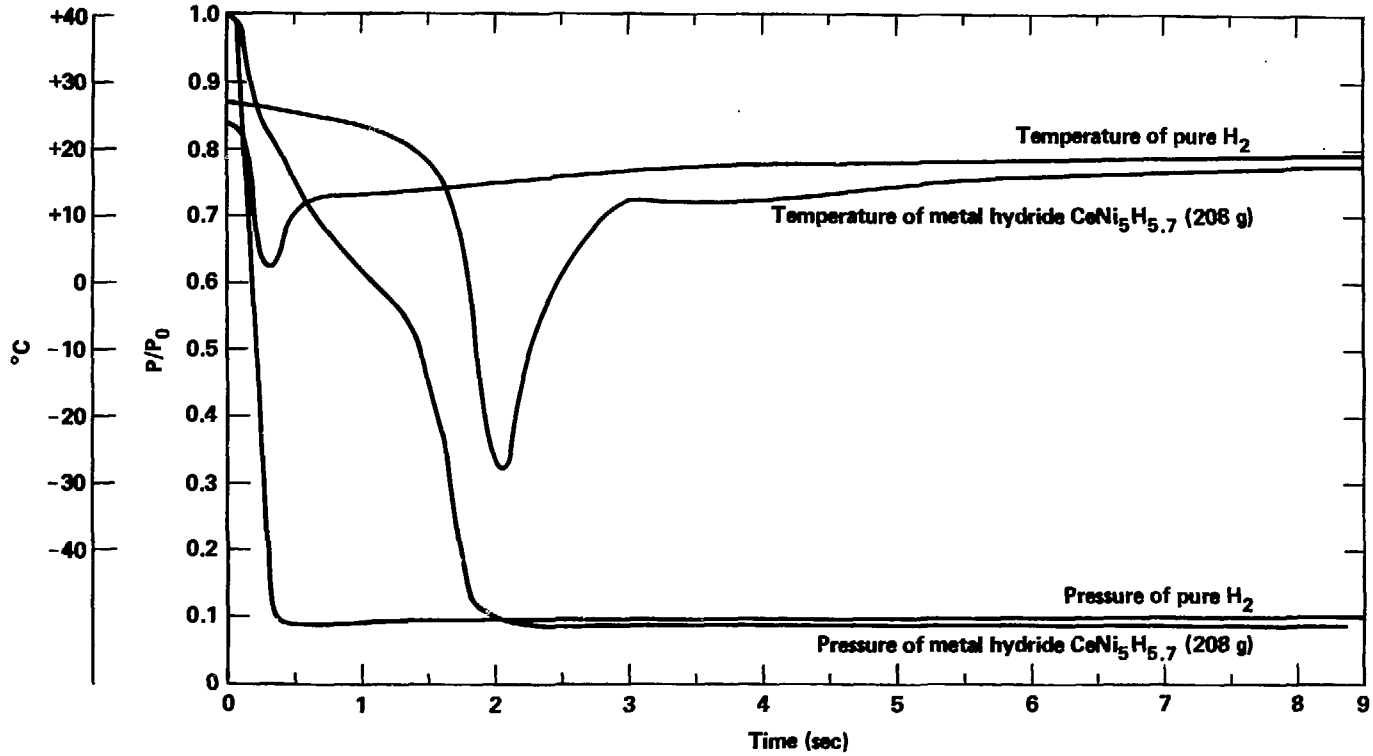

Figure 34. Pressure and temperature history in storage reservoir with receiving reservoir volume of 1026.5 cc.

Conclusions

The compounds studied in this report have the potential of supplying substantial hydrogen pressure at sub-zero temperatures. If the criteria are such that pressures were not substantial at low temperatures, auxiliary heat sources may be necessary to heat the hydride.

Our investigation showed that transferring hydrided $CeNi_5$ powder through tubing when the $CeNi_5$ was fully loaded with hydrogen at room temperature is feasible. Transfer tests with other hydrides may or may not behave in the same manner. Additional work is required on hydrides to satisfy engineering requirements. These are the following:

—Low- and high-temperature hydride transfer tests with deuterium and hydrogen.

—Determination of the rate of gas release for these hydrides (kinetics).

—Are the hydrides poisoned and by what means?

—Thermodynamic data, Cp, physical expansion data are needed for these hydrides.

—Determination of low-temperature isotherms to avoid extrapolation and to determine any abnormal behavior, e.g., $CeNi_5$ at $-21.5°C$.

—Investigation of the use of mixed hydrides and modifying existing hydrides.

—Investigation of hydrides which give less than substantial pressures at ambient and sub-zero temperatures for their behavior.

Acknowledgment

Thanks are given to Charles A. Slettevold for the particle-size analyses of the alloys and hydrided material.

References

1. H. H. Van Mal, "Stability of Ternary Hydrides of Some Applications," *Philips Res. Repts. Suppl.* No. 1, p. 1-88 (1976).
2. *Investigation of Hydriding Characteristics of Intermetallic Compounds*, University of Denver, Rept. DRI, LAR-55 (Nov. 15, 1961), DRI-2059 (Oct. 15, 1962).
3. H. W. Newkirk, *A Literature Study of Metallic Ternary and Quarternary Hydrides*, Lawrence Livermore National Laboratory, Livermore, CA, UCRL-52110 (August 2, 1976).

Ca-CaH_2

4. K. D. Becau, "The Use of Metal Hydrides for H_2 Storage in Automotive and Stationary Applications," in *Proc. 2nd International Congress, Hydrogen in Metals*, Paris, France, 6-10 June 1977, Vol. 3, pp. 1-8 6B.

La-LaH_2

5. K. D. Becau, "The Use of Metal Hydrides for H_2 Storage in Automotive and Stationary Applications," in *Proc. 2nd International Congress, Hydrogen in Metals*, Paris, France, 6-10 June 1977, Vol. 3, pp. 1-8 6B.

PuH_2

6. R. N. R. Mulford and G. E. Sturdy, "The Plutonium-Hydrogen System I. PuH_2 and PuD_2" *J. Amer. Chem. Soc.* **77**, 3449 (1955).

Li-LiH

7. K. D. Becau, "The Use of Metal Hydrides for H_2 Storage in Automotive and Stationary Applications," in *Proc. 2nd International Congress, Hydrogen in Metals*, Paris, France, 6-10 June 1977, Vol. 3, pp. 1-8 6B.

GdH_2

8. G. E. Strudy and R. N. R. Mulford, "The Gadolinum-H_2 System," *J. Amer. Chem. Soc.* **78**, 1084 (1956).

$MmNi_{4.5}Al_{0.5}$

9. E. L. Huston and G. D. Sandrock, "Engineering Properties of Metal Hydrides," *J. Less Common Metals* **74**, 435 (1980).

$MmNi_{4.5}Mn_{0.5}$

10. Y. Osumi, H. Suzuki, A. Kato, K. Ogaro, and M. Nakane, "The Development of Mischmetal Nickel and Titanium Cobalt Hydrides for Hydrogen Storage," *J. Less Common Metals* **74**, 271 (1980).

$LaNi_5$

11. E. L. Huston and G. D. Sandrock, "Engineering Properties of Metal Hydrides," *J. Less Common Metals* **74**, 435 (1980); also H. H. Van Mal, K. H. J. Buchow, and A. R. Miedima, "H_2 Absorption in $LaNi_5$ and Related Compounds," *J. Less Common Metals* **35**, 65, 76 (1974).

$Ca_{0.7}Mo_{0.3}Ni_5$

12. G. D. Sandrock, "A New Family of Hydrogen Storage Alloys Based on the System Nickel-Mischmetal-Calcium," in *12th Intersociety Energy Conversion Energy Conf.*, 1977, pp. 951-958.

FeTi-FeTiH

13. E. L. Huston and G. D. Sandrock, "Engineering Properties of Metal Hydrides," *J. Less Common Metals* **74**, 435 (1980).

NbH-NbH_2

14. R. H. Wiswall, Jr. and J. J. Reilly, *Inverse Hydrogen Isotope Effects in Some Metal Hydride Systems*, Brookhaven National Laboratory, Upton, NY, BNL-15859.

$CaNi_5$

15. E. L. Huston and G. D. Sandrock, "Engineering Properties of Metal Hydrides," *J. Less Common Metals* **74**, 435 (1980).

Pd-$PdH_{0.6}$

16. K. D. Becau, "The Use of Metal Hydrides for H_2 Storage in Automotive and Stationary Applications, in *Proc. 2nd International Congress, Hydrogen in Metals*, Paris, France, 6–10 June 1977, Vol. 3, pp. 1–8 6B.

Mg_2Cu-MgH_2 + $MgCu_2$

17. E. L. Huston and G. D. Sandrock, "Engineering Properties of Metal Hydrides," *J. Less Common Metals* **74**, 435 (1980); also K. D. Becau, "The Use of Metal Hydrides for H_2 Storage in Automotive and Stationary Applications, in *Proc. 2nd International Congress, Hydrogen in Metals*, Paris, France, 6–10 June 1977, Vol. 3, pp. 1–8 6B.

Mg_2Ni-Mg_2NiH_4

18. E. L. Huston and G. D. Sandrock, "Engineering Properties of Metal Hydrides," *J. Less Common Metals* **74**, 435 (1980); also K. D. Becau, "The Use of Metal Hydrides for H_2 Storage in Automotive and Stationary Applications, in *Proc. 2nd International Congress, Hydrogen in Metals*, Paris, France, 6–10 June 1977, Vol. 3, pp. 1–8 6B.

Mg-MgH_2

19. E. L. Huston and G. D. Sandrock, "Engineering Properties of Metal Hydrides," *J. Less Common Metals* **74**, 435 (1980).

$MmNi_5$

20. Y. Osumi, H. Suzuki, A. Kato, K. Ogaro, and M. Nakane, "The Development of Mischmetal Nickel and Titanium Cobalt Hydrides for Hydrogen Storage," *J. Less Common Metals* **74**, 271 (1980).

90V-10Cr

21. Y. Osumi, H. Suzuki, A. Kato, K. Ogaro, and M. Nakane, "The Development of Mischmetal Nickel and Titanium Cobalt Hydrides for Hydrogen Storage," *J. Less Common Metals* **74**, 271 (1980).

$CeNi_5$

22. Molycorp, Inc., *Overview of Metallurgical Application Data and Ideas*, Bulletin No. 56, White Plains, New York 12M-4-77.

YCo_5

23. T. Takeshita, W. E. Wallace, and R. S. Craig, "Hydrogen Solubility in 1:5 Compounds Between Thorium and Nickel and Cobalt," *Inorganic Chem.* **13** (9), 282 (1974).

VH-VH_2

24. R. H. Wiswall, Jr. and J. J. Reilly, "Inverse Hydrogen Isotope Effects in Some Metal Hydride Systems," *J. Amer. Chem. Soc.* **81**, 5019 (1959). [also available as Brookhaven National Laboratory report BNL-15895]

$TiCr_{1.9}H_{2.63}$

25. J. R. Johnson, "Reaction of Hydrogen with the High Temperature Form of $TiCr_2$," *J. Less Common Metals* **73**, 345 (1980).

$Ca_{0.2}Mm_{0.8}Ni_5$

26. E. L. Huston and G. D. Sandrock, "Engineering Properties of Metal Hydrides," *J. Less Common Metals* **74**, 435 (1980).

$MmNi_{4.5}Cr_{0.5}$
27. Y. Osumi, H. Suzuki, A. Kato, K. Ogaro, and M. Nakane, "The Development of Mischmetal Nickel and Titanium Cobalt Hydrides for Hydrogen Storage," *J. Less Common Metals* **74**, 271 (1980).

$MmNi_5$
28. E. L. Huston and G. D. Sandrock, "Engineering Properties of Metal Hydrides," *J. Less Common Metals* **74**, 435 (1980).

$La_{0.67}Nd_{0.25}Pr_{0.08}Ni_5$
29. Molycorp, Inc., *Overview of Metallurgical Application Data and Ideas*, Bulletin No. 56, White Plains, New York 12M-4-77.

$LaNi_4Cu$
30. J. J. Reilly and R. H. Wiswall, Jr., Hydrogen Storage and Purification Systems, Brookhaven National Lab., Upton, New York, BNL 17136 (August 1, 1972).

$Nb_{0.5}V_{0.5}$
31. J. J. Reilly and R. H. Wiswall, Jr., "The Higher Hydrides of V and Nb," *Inorganic Chem.* **9** [7], 1678 (1970).

$Zr(Co_{0.5}Mm_{0.5})_2H_{3.1}$
32. D. Shaltiel, I. Jacob, D. Davidov, "Hydrogen Absorption and Desorption Properties of AB_2 Laves—Phase Pseudobinary Compounds," *J. Less Common Metals* **117**, 131 (1977).

$Zr(Fe_{0.75}Cr_{0.25})_2H_{2.85}$
33. Molycorp, Inc., *Overview of Metallurgical Application Data and Ideas*, Bulletin No. 56, White Plains, New York 12M-4-77.

$Ti_{0.4}Mm_{0.6}H_{0.9}$
34. T. Yamashita, et al., *Nippon Kinzoku Gakkaishi* **42**, 148 (1977).

66.34 wt% $LaNi_5$ + $Ti_{0.8}Zr_{0.2}Cr_{0.8}Mm_{1.2}$
35. S. Suda and M. Uchida, "Mixing Effects of Two Different Types of Hydrides," *Proc. International Symposium, Hydrides for Energy Storage*, Geilo, Norway, Aug. 14–19, 1977, pp. 515-525.

$MmNi_{4.15}Fe_{0.85}$
36. E. L. Huston and G. D. Sandrock, "Engineering Properties of Metal Hydrides," *J. Less Common Metals* **74**, 435 (1980).

$TiCr_{1.9}H_{3.19}$
37. J. J. Reilly and R. H. Wiswall, Jr., *Hydrogen Storage and Purification Systems*, Brookhaven National Lab., Upton, New York, BNL-17136 (August 1, 1972).

38. H. H. Van Mal, K. H. J. Buschow, and A. R. Miedima, "Hydrogen Absorption in $LaNi_5$ and Related Compounds: Experimental Observations and Their Explanations," *J. Less Common Metals* **35**, 65 (1974).
39. G. D. Sandrock, "Development of Low Cost Alloys Based on the Nickel-Mischmetal-Caicium System," *12th Intersociety Energy Conversion Energy Conf.*, Washington, D.C. 1977, Vol. 1., Amer. Nuclear So., LaGrange Park, Illinois, 1977, p. 951.
40. C. E. Lundin and F. E. Lynch, *Proc. International Symp. of Hydrides for Energy Storage*, Geilo, Norway, 1977 (Pergamon Press, Oxford, 1978), pp. 395–403.
41. F. A. Kiujpers and B. D. Loopstra, *J. Phys.* (suppl) **32**, C-1-657 (1971).
42. D. Dayan and M. P. Dariel, "Hysteresis Effects in Cerium-Containing $LaLi_5$ Type Compounds," *J. Less Common Metals* **73**, 15 (1980).

43. Molycorp, Inc., *Overview of Hydrogen Sponge Alloys*, Bulletin No. 56, White Plains, New York.
44. L. Huston, Ergenics, Wyckoff, N.J., private communication, 1982.
45. G. D. Sandrock, "The Metallurgy and Production of Rechargeable Hydrides," in: Proc. of an International Symposium, Hydrides for Energy Storage, Geilo, Norway, Aug. 14–19, 1977 p. 353 (Pergamon Press: Oxford, 1978).
46. S. Suda and M. Uchida, "Mixing Effects of Two Different Types of Hydrides," *Proc. of an International Symposium*, Geilo, Norway, Aug. 14–19, 1977 (Pergamon Press: Oxford, 1978).
47. J. H. Potter and M. J. Levy, "The Free Expansion of Dry and Moist Air," *Journal of Engineering for Ind., Trans. of ASME*, pp. 97–100, Feb. 1961.

Appendix

The curves shown in the appendix, Figs. 35 and 36 represent Van't Hoff hydride isochores from several sources. The sources are listed in the reference section corresponding to the numbers on the curves.

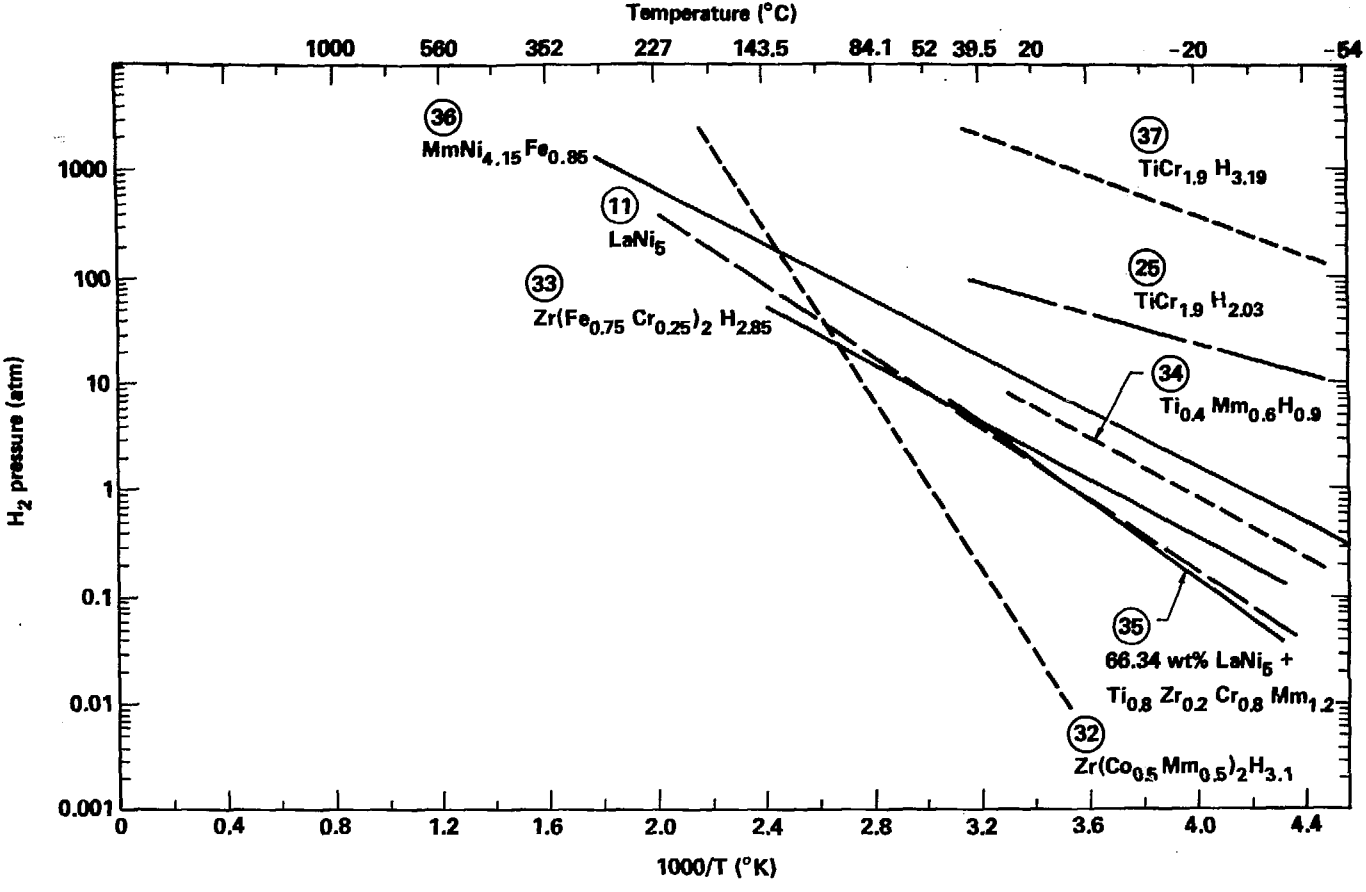

Figure 35. Van't Hoff plots (desorption) for various hydrides.

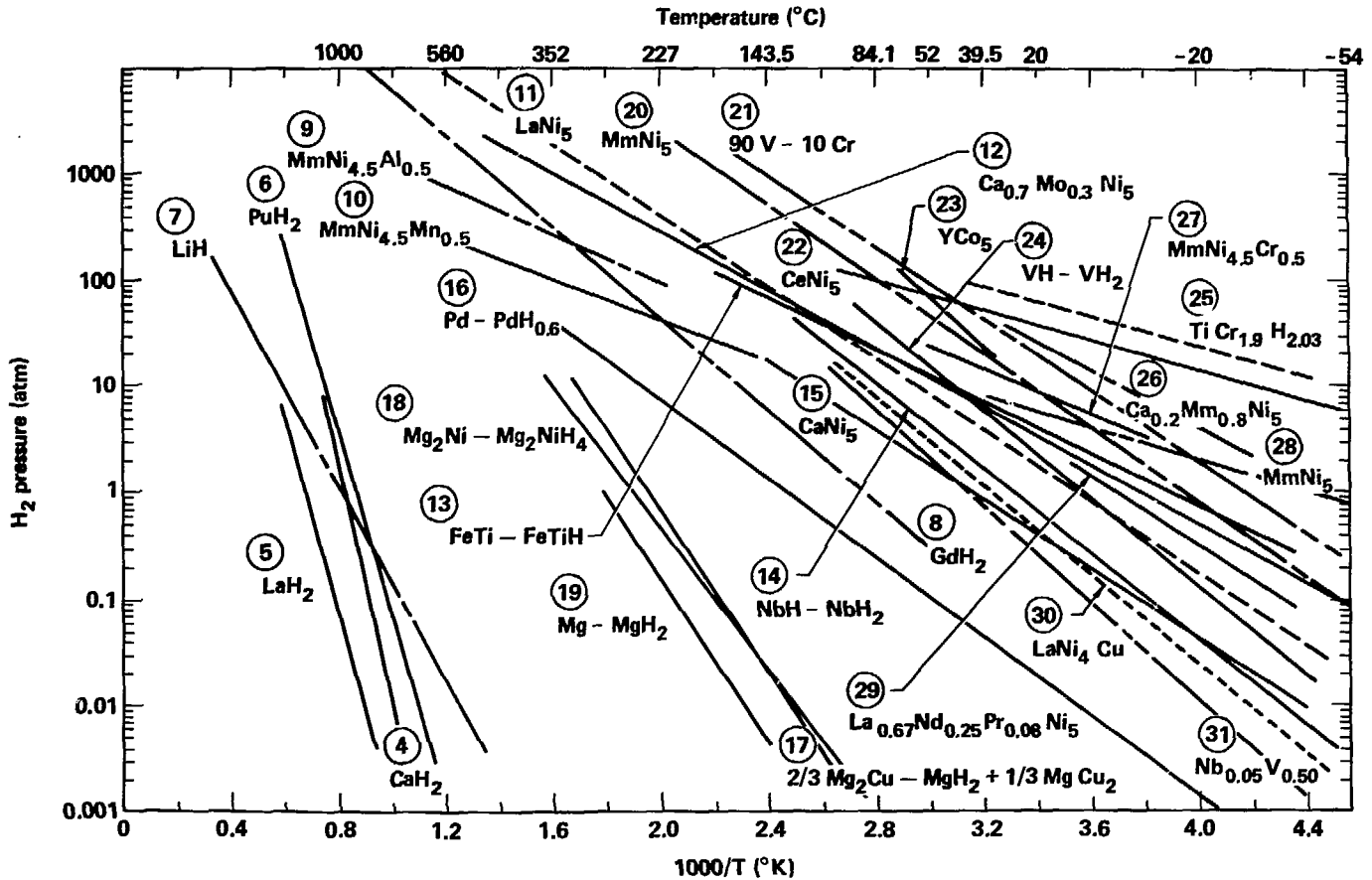

Figure 36. Van't Hoff (desorption) for various hydrides (isochores). Because most isotherms slope, a formula is indicated on each Van't Hoff plot. if no formula is indicated, the Van't Hoff plot was determined at plateau midpoint (circled numbers refer to references listed at the end of this report).